Title: Effect of the surface polarity, through employing nonpolar spacer groups, on the glass-transition dynamics of poly(phenyl methylsiloxane) confined in alumina nanopores

Author: Roksana Winkler, Wenkang Tu, Mateusz Dulski, Łukasz Laskowski, Karolina Adrjanowicz

Citation style: Winkler Roksana, Tu Wenkang, Dulski Mateusz, Laskowski Łukasz, Adrjanowicz Karolina. (2021). Effect of the surface polarity, through employing nonpolar spacer groups, on the glass-transition dynamics of poly(phenyl methylsiloxane) confined in alumina nanopores. "Macromolecules" (2021), no. 0, s.1-18. DOI: 10.1021/acs.macromol.1c02145

Macromolecules

pubs.acs.org/Macromolecules

Article

Effect of the Surface Polarity, Through Employing Nonpolar Spacer Groups, on the Glass-Transition Dynamics of Poly(phenyl methylsiloxane) Confined in Alumina Nanopores

Roksana Winkler,* Wenkang Tu, Mateusz Dulski, Lukasz Laskowski, and Karolina Adrjanowicz*

Cite This: https://doi.org/10.1021/acs.macromol.1c02145

Read Online

ACCESS | Metrics & More | Article Recommendations | Supporting Information

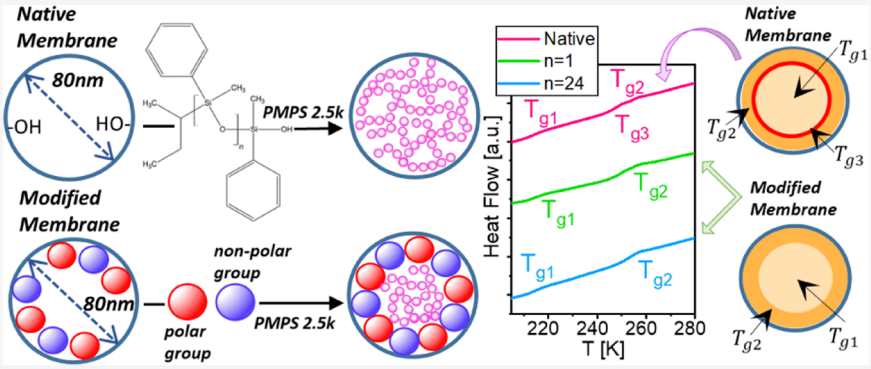

ABSTRACT: Broadband dielectric spectroscopy and differential scanning calorimetry were used to study the effect of changes in the surface conditions on the segmental dynamics of poly(phenylmethylsiloxane) confined in alumina nanopores. Functionalization was done using highly polar propyl phosphoric units separated by the assumed concentration of triethoxysilane groups (from $N = 0$ to $N = 24$). By adjusting the proportion between polar units and nonpolar spacers, it was possible to control the surface polarity. Modification of the surface conditions does not inhibit the formation of the adsorbed layer, as revealed by the presence of two T_g's in calorimetric results. However, changes in the surface polarity will prevent the growth of the additional interlayer in between the core volume and the interfacial layer. Finally, we also found that the changes in the surface polarity affect the equilibration kinetics and can be used to control the time scale of the structural recovery toward the equilibrium state.

INTRODUCTION

Understanding polymers' behavior at the nanoscale level is a subject of continuous research due to the numerous applications of polymer materials in microelectronic devices, solar cells, smart coatings, nanocomposites, and many others.[1−5] The interest in nanoscale phenomena is because when the size available for the polymer chain mobility approaches that of finite length, its dynamic and static properties can drastically change compared to what we usually term a "bulk". In turn, confinement is a unique state when the intrinsic properties of the polymer material depend on the sample thickness or imposed geometrical constraints.

In nanoscale confinement, a material's characteristic properties are dominated by the finite size effect and interactions with the interfaces or confining surfaces.[6−11] In thin polymer films supported by a solid substrate, the finite size effect affects the relaxation dynamics, the glass-transition temperature, the physical aging behavior of the glassy polymer, or the chain conformation.[12−16] Likewise, by infiltrating the polymer sample inside cylindrical nanopores, its static and dynamic properties may also change. For example, when lowering the pore size, the glass-transition temperature can decrease or remain unchanged compared to the bulk value.[9,10,17−19] In addition, the α-relaxation process, associated with segmental mobility, broadens and its strength decreases.[6−8]

On the other side, the surface effects also have an enormous impact on the polymer's dynamics.[9,20−28] Strong attractive interactions can lead to the adsorption of the polymer segments on the surface by forming hydrogen bonds. This produces a gradient in dynamics across the film or nanopores, resulting in more than one glass-transition event in a confined geometry. The fraction of the polymer chains anchored to the solid substrate has reduced mobility compared to the bulk polymer. Conversely, those located away from the supported surfaces are weakly or entirely not affected by confinement.

Received: October 14, 2021
Revised: October 26, 2021

Strong interactions at the polymer−substrate interface results also in the local density distribution that vanishes when moving away from the confining surface. In turn, at the free surface, the polymer chains reveal enhanced mobility orders of magnitude faster than the bulk dynamics.

It is often claimed that glass-transition dynamics in the confined state is the outcome of the counterbalance between finite size and surface effects.[6,21,29,30] In addition, in some cases, with the reduction of the thickness, the influence of the finite size effect can be overpowered by the substrate interaction. For this reason, understanding how the surface conditions affect the behavior of polymers and glass-forming systems at the nanoscale is an active research topic.[9,20,22,31−33]

However, the picture of the nanoscale-confinement phenomena seen only as the interplay between the finite size and surface effects is not complete. In recent years, the growing number of experimental evidence points out that the soft matter confined at the nanoscale level is trapped in an out-of-equilibrium state. In such conditions, it can reside for a very long time.[34] The effects seen in confined geometry depend on the thermal history or the processing conditions.[35−40] When provided enough time, confined material can reach the equilibrium configuration and therefore reduce or even eliminate some of the striking features seen only in constrained geometry.[28,34−36,41−43] In thin films, upon prolonged annealing, the conformation of the polymer chains located close to the substrate is changing due to increased irreversible adsorption.[41,43−48] Prolonged annealing can slow down initially faster dynamics as observed in thin films of poly(methylmethacrylate) and poly(vinyl acetate).[42] Plus, it can restore some of the bulk sample's properties, such as T_g and dielectric strength.[41,43−48] Likewise, in nanopore confinement, one can observe out-of-equilibrium phenomena.[35−39] One of them is the ability to recover by the system some of the bulk properties, such as the temperature evolution of the α-relaxation time.[35,36] Upon annealing, the polymer chain packing density changes and slows down the segmental dynamics.[35,36]

One of the strategies that can be used to alter the surface effects originating from the interaction of the polymer with the pore walls is the chemical substitution of the surface-anchored hydroxyl groups by various organosilanes. Numerous experimental studies demonstrate that the change in the surface chemistry due to silanization affects the structure of the interfacial and core layers,[22] the glass-transition temperature,[20] and increases the hydrophobicity of the surface.[9,20,23,32,33] Moreover, due to silanization, the effect of confinement may be partially or completely removed,[32,49−51] or either become more pronounced when the pore diameter is reduced accordingly.[50,51] The efficiency of the silanization procedure depends on the silanizing agent that is used. For example, alkylsilanes are more effective in changing the glass-transition behavior as compared to fluorosilanes.[20] However, the surface modification strategies do not involve only silanization; there are other methods, for example, the use of ODPA (octadecylphosphonic acid), which may affect the crystallization and local dynamics of nanopore-confined poly(ε-caprolactone),[52] as well as control the phase behavior of liquid-crystalline materials.[53] Apart from that an atomic-layer-deposition technique can be utilized to fine-tune the surface properties of the confined nanomaterials.[31]

Depending on the silanization procedure, which is used to modify the surface of the nanopores, the formation of the adsorbed layer, as well as the segmental mobility, might be quite different. This we have demonstrated recently for poly(phenylmethylsiloxane) confined in alumina membranes with surface modification using two different silanization agents, chlorotrimethylsilane (ClTMS) and (3-aminopropyl)-trimethoxysilane (APTMOS).[28] ClTMS was responsible for replacing the native hydroxyl groups with trimethylsilane units, while APTMOS provides aminopropylsilane species at the pore surface. Such a distinct change turned out to have a significant impact on the temperature evolution of the segmental relaxation time and the breadth of the relaxation function. Nevertheless, both silanization agents do not inhibit the formation of the interfacial layer, as the two glass-transition events were still detected on DSC thermograms of the confined polymer.

When it comes to aluminum oxide surfaces, silanization is less effective in creating homogeneous nonpolar (hydrophobic) surfaces than in the case of hydroxylated silica surfaces. In turn, the use of phosphonic acid on alumina surfaces gives more ordered self-assembled monolayers.[53] For this reason, in this work, we have modified the surface of cylindrical alumina nanopores using highly polar phosphonic acid units that were separated using the assumed concentration of nonpolar spacer units. The pore diameter remains fixed, 80 nm. The use of spacer groups allowed for the compatible distribution of the polar functional units.[54] Because the spacer units were nonpolar, adjusting the proportions between the polar functional units and nonpolar spacers has enabled us to precisely control the polarity of the surface. With the use of such functionalized alumina nanopores, we have aimed to investigate the segmental dynamics of the studied polymer, poly(phenylmethylsiloxane), denoted PMPS 2.5k. The choice of the tested material was as followed. At first, from the previous study, we know that the glass-transition dynamics of PMPS 2.5k is very sensitive to small frustration in density, and therefore also confinement effects. Second, by comparing with the previous results focused on ClTMS- and APTMOS-treated nanopores, we can evaluate the influence of the different strategies used to modify the chemistry of the pore walls on the glass-transition dynamics in a confined space. Introducing hydrophobic conditions at the surface turned out to affect various aspects of the confined polymer dynamics. This includes, for example, preventing the formation of the third molecular layer, "interlayer", located in between the adsorbed layer and core volume. Functionalization of the pore surface with the alternate use of polar/nonpolar units also affects the equilibration kinetics and can be used to tune the time scale of the structural recovery. Surprisingly, irrespective of the surface conditions or thermal treatment protocol, we were still able to detect two glass-transition events in calorimetric response of the confined polymer. They are typically attributed to chain mobility close to the pore walls and center of the pores. The values of both T_g's shift slightly toward higher temperatures with increasing the surface polarity and after annealing. Nevertheless, they are still present. Results of the dielectric relaxation and differential scanning calorimetry (DSC) studies demonstrate that taming the surface conditions could help to get a better understanding and control over the behavior of confined polymer materials in nonequilibrium states.

EXPERIMENTAL SECTION

Materials. The tested polymer is poly(phenylmethylsiloxane) labeled in the text PMPS 2.5k, with M_n = 1 800, and polydispersity

https://doi.org/10.1021/acs.macromol.1c02145
Macromolecules XXXX, XXX, XXX−XXX

index (PDI) = 1.40. We show the chemical structure of PMPS in Figure 1. The sample was purchased from Polymer Source Inc.

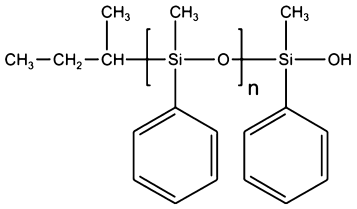

Figure 1. Chemical structure of poly(phenylmethylsiloxane) used in this study.

(Canada) as a clear, viscous, transparent liquid and used without further purification. The glass-transition temperature of bulk PMPS 2.5k determined from the dielectric spectroscopy (DS) measurements is T_g = 230 K ($T_g = T$ at which τ_α = 1 s), while that from the DSC, we get T_g = 230.3 K.[28,55] Numerous studies report the T_g value for bulk PMPS to increase with the molecular weight.[56−60] For M_n = 2 200 and PDI 1.28, Alexandris et al. obtained T_g = 229 K (DS) and T_g = 228 K (DSC).[56]

AAO Templates and Method of Infiltration. *Native AAO Nanopores.* We have used commercially available anodized aluminum oxide membranes (pore diameter of 80 ± 6 nm, pore depth 100 ± 1 μm) purchased from InRedox. The membranes are composed of uniform hexagonal pore arrays aligned perpendicular to the surface of the material and penetrating its entire thickness. The pore channels are aligned parallel to each other. The diameter of the alumina membrane is 13 ± 0.2 mm. The porosity of anodized alumina oxide (AAO) membranes is 13%. Before filling, AAO membranes were dried at 433 K in a vacuum oven for 24 h to remove any volatile impurities from the nanochannels. In the next step, PMPS was placed on the top of the AAO membranes, and then the entire system was kept at T = 313 K under vacuum for 2 weeks. This allows the liquid to flow inside the nanopores by capillary forces. The membranes were weighed before and after infiltration. We have assumed that the filling is completed once the mass of the membrane ceases to increase with time. Then, the surface of the membranes was dried using delicate dust-free tissues. Typically, the polymer mass inside 80 nm AAO membranes varies within 2.1−2.5 mg.

Chemical Modification of the Pore Surface. For pore surface modification, we have used AAO membranes (InRedox) characterized by the same paraments as described above. We have prepared the functionalized porous AAO matrices containing highly polar propyl phosphoric acid units with an assumed concentration at the surface. The use of spacer groups allowed to tune the distribution of the polar functional units.[54] Taking into consideration that the spacer units are nonpolar, we can control the polarity of the surface by adjusting the proportions between the polar functional units and nonpolar spacers. The visual presentation of the material and the idea of using spacer units can be seen in Figure 2.

We have prepared a few samples for the investigation, containing various proportions between the polar and nonpolar units, so the various polarity of the surface. We assumed that these would be the representative samples, containing 0, 1, 3, 6, 12, and 24 nonpolar spacers per single polar phosphonic acid unit. Samples were named AAO−$PO(OH)_2$−NX, where X denoted the number of spacers per individual polar unit. Functionalization of the AAO matrices was carried out under an argon atmosphere using a vacuum line. Solvents were dried out and distilled just before the use. Reagents with the highest available purity were used for reactions. Chlorotrimethoxysilane (ClTMS), bromotrimethoxysilane (BrTMS), and tetraethylorthosilicate (TEOS) were purchased from Sigma-Aldrich and used as supplied. Phosphonatepropyltriethoxysilane, hereafter called PPTES, was purchased from Syntal Chemicals. The schematic presentation of the functionalization procedure can be seen in Figure 3.

Before the functionalization process, we have dried AAO matrices under vacuum at a temperature of 150 °C for 24 h to remove any excess water from the pores. Such prepared matrices underwent the procedure of grafting by precursors of the polar functional units and precursors of the nonpolar spacer units (STEP 1). Here, we have defined the assumed surface polarity but setting the molar proportions between dopants: TEOS and PPTES. To do this, measured amounts

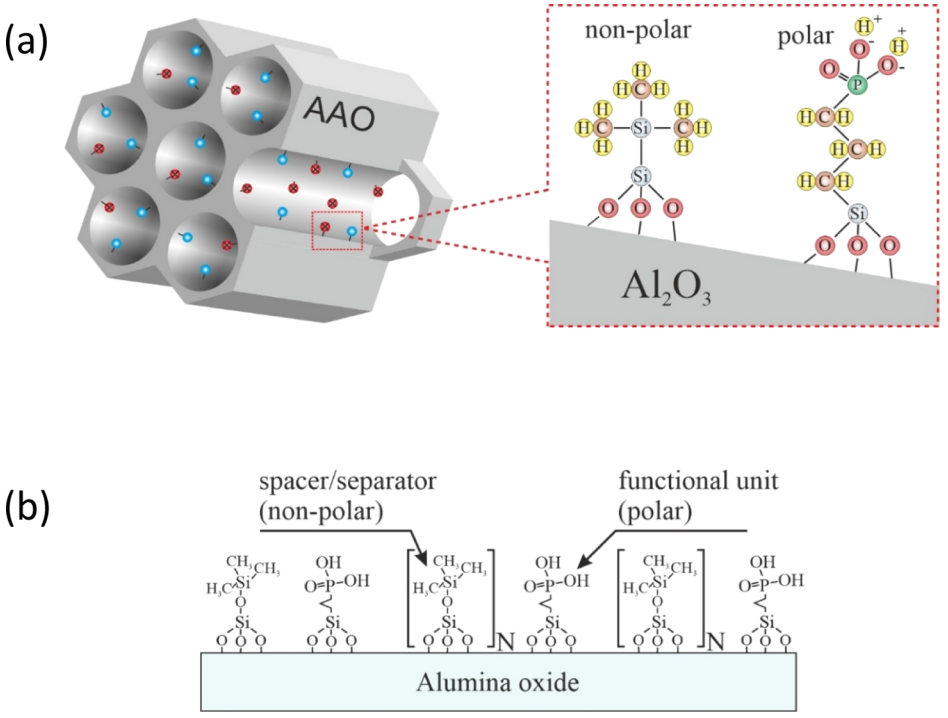

Figure 2. Visualization of the AAO templates (a) and concept of tuning surface polarity using nonpolar spacer units. (b) Number of N determines the molar proportion between polar (phosphonic acid) and nonpolar (trimethoxysilane) units and the total polarity of the surface.

https://doi.org/10.1021/acs.macromol.1c02145
Macromolecules XXXX, XXX, XXX−XXX

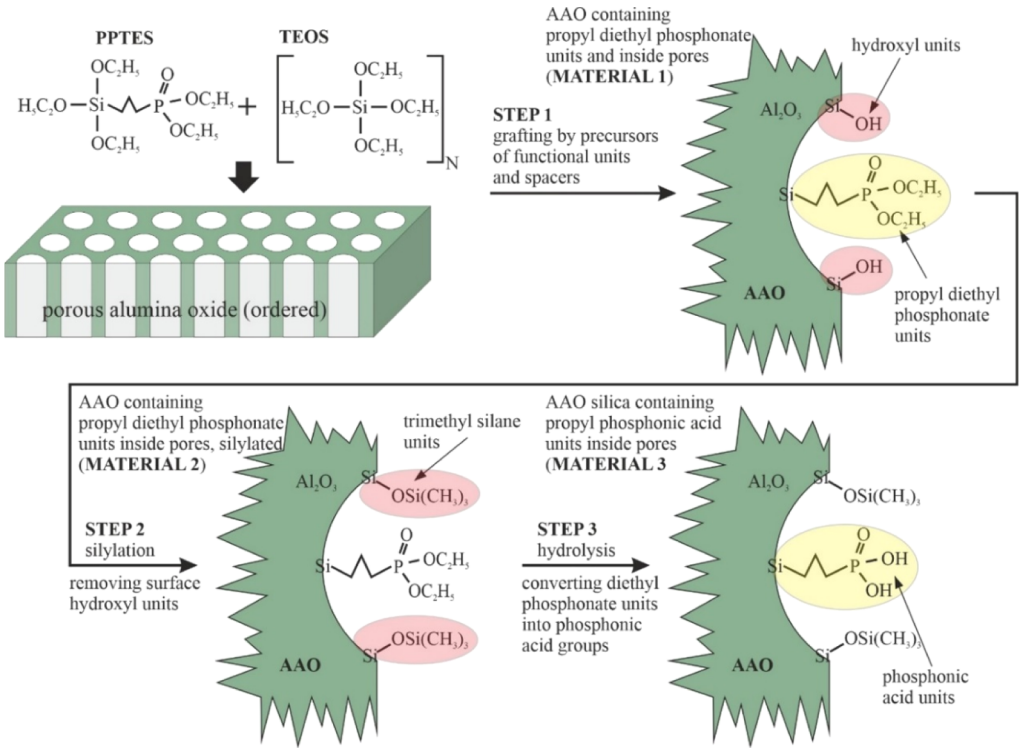

Figure 3. Visualization of the functionalization procedure for porous alumina oxide matrices using phosphonic acid units separated by trimethyl silane.

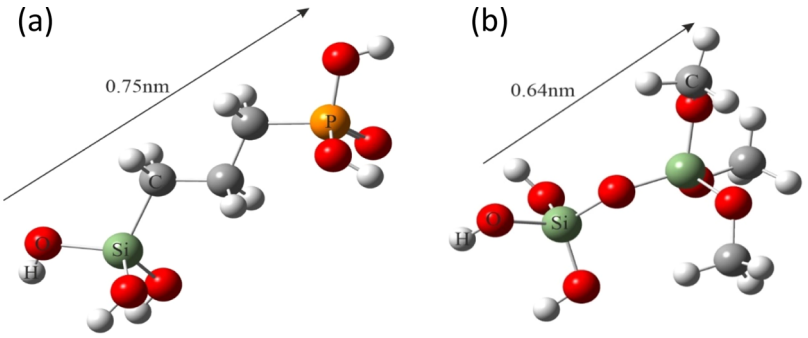

Figure 4. Geometrically optimized models of the functional units ($(-O)_3-Si-(CH_2)_3-PO(OH)_2$)—(a) and spacer groups ($(-O)_3-Si-O-Si(O-CH_3)_3$)—(b) with the diagonal line which marks the total lengths.

of TEOS and PPTES were mixed in toluene (4% solution) for 2 h under argon. We have prepared five solutions, which contained various concentrations of the TEOS and PPTES: 0:1 (total functionalization, with no spacers), 1:1; 3:1; 6:1; 12:1, and 24:1 (final samples: AAO−$PO(OH)_2$−N0, AAO−$PO(OH)_2$−N1, AAO−$PO(OH)_2$−N3, AAO−$PO(OH)_2$−N6, AAO−$PO(OH)_2$−N12, and AAO−$PO(OH)_2$−N24). Completely dried AAO matrices were inserted into open teflon par-autoclaves, and the grafting solutions were immediately poured. Samples were degassed under a vacuum to ensure the total filling of the pores by the solution. Next, autoclaves were closed and kept untouched for 24 h at a temperature of 80 °C. After this time, the samples were rinsed with toluene, immersed in the pure toluene again, and put into an ultrasonic bath for 1 h to remove any excess of the doping solution and avoid its polymerization. We have repeated the procedure twice for toluene and once for dichloromethane. Afterward, the samples were dried in a vacuum overnight inside open teflon autoclaves, ready for the subsequent processing. The obtained AAO matrices contain esters of phosphonic acid and surface hydroxyl units in assumed proportions. In STEP 2, hydroxyl units were transferred into nonpolar triethoxy units by silanization. This was achieved by treating the pre-functionalized AAO matrices with a solution of chlorotrimethylsilan in toluene (2% of volume). The procedure was the same as in the previous step. Also, here we have carried out the reaction in closed teflon-par autoclaves at a temperature of 80 °C for 24 h. We have washed the samples in the same way as previously. We have applied a selective two-step process to hydrolyze (STEP 3) the phosphonic acid diethyl ester groups into phosphonic acid. This was done by treating the samples with a solution of bromotrimethylsilane in toluene (4% of volume) in the same way as in the previous steps. After washing and drying samples, they were immersed in a mixture of methanol and deionized water (1:1 of volume) to complete the conversion. The resulting samples containing phosphonic acid units separated by triethoxysilane groups in assumed proportions were dried under vacuum and stored in a protective atmosphere of argon. The detailed characterization of the modified alumina surfaces and verification of each synthesis step can be found in the Supporting Information.

METHODS

Water Contact Angle. In order to characterize the surface properties of the modified alumina substrates, we have measured the water contact angle (WCA) using a drop shape analysis instrument

https://doi.org/10.1021/acs.macromol.1c02145
Macromolecules XXXX, XXX, XXX−XXX

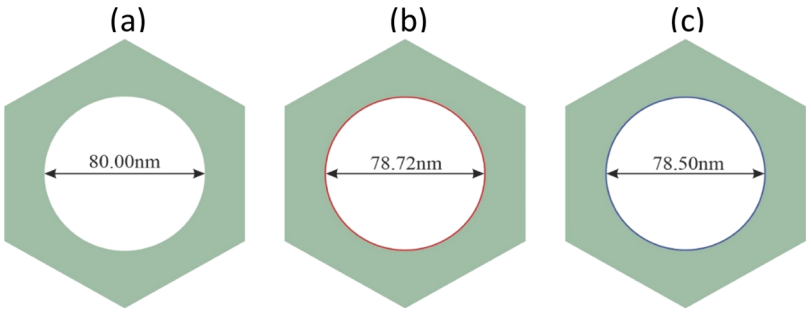

Figure 5. Visualization of the influence of functionalization on the narrowing of the pore channels with a diameter of 80 nm. The borderline cases were considered: nonfunctionalized AAO matrix (a) AAO matrix functionalized exclusively with spacer units (spacer units layer was red marked—(b)) and AAO matrix functionalized exclusively with functional units (functional units layer was blue marked—(c)).

(JC2000D contact angle tester) under ambient humidity and temperature. We have applied the sessile drop technique for the measurement of static contact angle. We have used 5 μL of deionized water in each drop. The contact angle was measured immediately after dropping H_2O. For all samples, we have checked the variation in the contact angle with time by taking an additional measurement after 30 s from the dropping. There was no significant difference in the case of the reference material (pure, unfunctionalized AAO matrix). For functionalized alumina, the contact angle was constant in time.

Geometry of the Nanopores. To check the geometry of the functional units and spacer groups, we have prepared their numerical models and optimized them geometrically. Theoretical calculations were carried out in the gas phase using the density functional theory calculations[61] available in the Gaussian 09 software package.[62] The geometry of the modeled molecules was first optimized using the Becke's hybrid exchange and correlated three-parameter[63] with the Lee–Yang–Parr correlation functional (B3LYP),[64] and the split-valence basis sets 3-21G. Next, the optimized structures were used as input files for further optimization and the vibrational harmonic calculations using the MOLPRO Basis Query def2-TZVP,[65] as a reasonably accurate basis set within a reasonable computational time. As a result of the geometry optimization, we had obtained a few conformers for each molecule. The final configurations of the models were selected based on the conformational analysis. Conformers with the lowest energy had been chosen as the correct ones.

The numerical simulations allow for the estimation of the lengths of the functional and spacer units, thus estimating their impact on the pores' volume. The structures of the optimized molecules, and their sizes are shown in Figure 4. As can be seen, the lengths of the spacer units and functional groups are significantly lower than the diameter of the pores (80 nm). Thus, in our opinion, their impact on the pores' volume can be negligible.

The channel interior is covered with functional units and separator groups with variable proportions. One can consider some narrowing of the diameter of the pores as a result of such functionalization. The approximated length of the functional unit is 0.75 nm, while the spacer group has 0.64 nm (see: Figure 4). Considering that the diameter of the pores is 80 nm, the narrowing resulting from the functionalization is negligible. Moreover, the difference in the diameter of the functional and spacer units is only 0.11 nm, and the influence of the proportions between the spacers and functionalities cannot be seen practically. Figure 5 visualizes this situation. As can be seen, the narrowing of the pores is much lower than the error in measuring the pore sizes after the synthesis of the AAO matrix and the variation in the diameter of the channels. Likewise, the radius of gyration for the studied polymer (PMPS of M_n = 1800) is less than 1.5 nm (~1.43 nm), meaning that it is much smaller than the diameter of the considered nanopores (80 nm). Therefore, $2R_g/D$ is 0.0356.[66]

Dielectric Spectroscopy. DS measurements for bulk and nanopore-confined PMPS were made with a Novocontrol Alpha frequency analyzer. For the bulk sample, we have used standard plate–plate electrodes of 20 mm in diameter separated by a 50 μm teflon spacer. Native and surface-modified alumina nanopores filled with the investigated polymer were placed between two round electrodes with a diameter of 10 mm. Bulk and nanopore-confined samples were measured as a function of temperature in the frequency range from 10^{-2} to 10^6 Hz. The temperature was controlled with stability better than 0.1 K by a quatro system. The complex dielectric permittivity $\varepsilon^* = \varepsilon' - i\varepsilon''$, where ε' is the real and ε'' is the imaginary part, were collected on (i) slow cooling with 0.2 K/min from 293 to 219 K and (ii) slow heating from 219 to 293 K with 0.2 K/min followed by fast quench (10 K/min). The time-dependent measurements were also carried out using a Novocontrol Alpha analyzer for up to 20 h at different temperatures. Thermal protocol for such experiments involved quenches from the room temperature to an intermediate temperature or either directly to a selected annealing temperature.

Because the nanopore-confined material reveals strongly non-equilibrium behavior, the polymer samples have experienced exactly the same thermal treatment and time-interval protocols. The dielectric measurements were performed immediately after weighting and cleaning the surface of the nanoporous templates. Recently, Tu and co-workers have dwelled on that subject more carefully and demonstrate that the intensity of the dielectric loss curve for *cis*-1,4-polyisoprenes in AAO templates changes after complete imbibition. Interestingly, it can even completely reverse the trend due to increasing adsorption. As a result, the dielectric loss curves start to decrease in intensity with time.[67,68]

Analysis of the Dielectric Permittivity for the Polymer Confined in Alumina Nanopores. Herein, it should be noted that the nanopore-confined system under consideration is an inhomogeneous dielectric that includes the tested polymer located inside the alumina matrix. Because the electric field runs along the nanopore channels, the entire heterogeneous dielectric response problem can be modeled using the equivalent circuit composed of the two capacitors connected in parallel. In such a case, the dielectric permittivity of a composite material (the raw data that we measure using an impedance analyzer) is the sum of the dielectric permittivity of the individual components—confined polymer and alumina matrix—weighted by the respective volume fractions[69]

$$\varepsilon_{composite} = \varepsilon_{polymer}\varphi + (1 - \phi)\varepsilon_{AAO} \quad (1)$$

where φ is the porosity of the alumina membrane, ε_{AAO} is the dielectric permittivity of the alumina membrane, and $\varepsilon_{polymer}$ is the dielectric permittivity of the confined polymer. Thus, for the real and imaginary parts, we get

$$\varepsilon'_{polymer} = \frac{\varepsilon'_{composite} - \varepsilon_{AAO}(1 - \varphi)}{\varphi}$$

$$\varepsilon''_{polymer} = \varepsilon''_{composite}/\varphi \quad (2)$$

To characterize the dielectric permittivity of the matrix, we have measured the dielectric signal of the empty AAO membranes. The data presented in Figure 6a show that the values of ε' are almost

https://doi.org/10.1021/acs.macromol.1c02145
Macromolecules XXXX, XXX, XXX–XXX

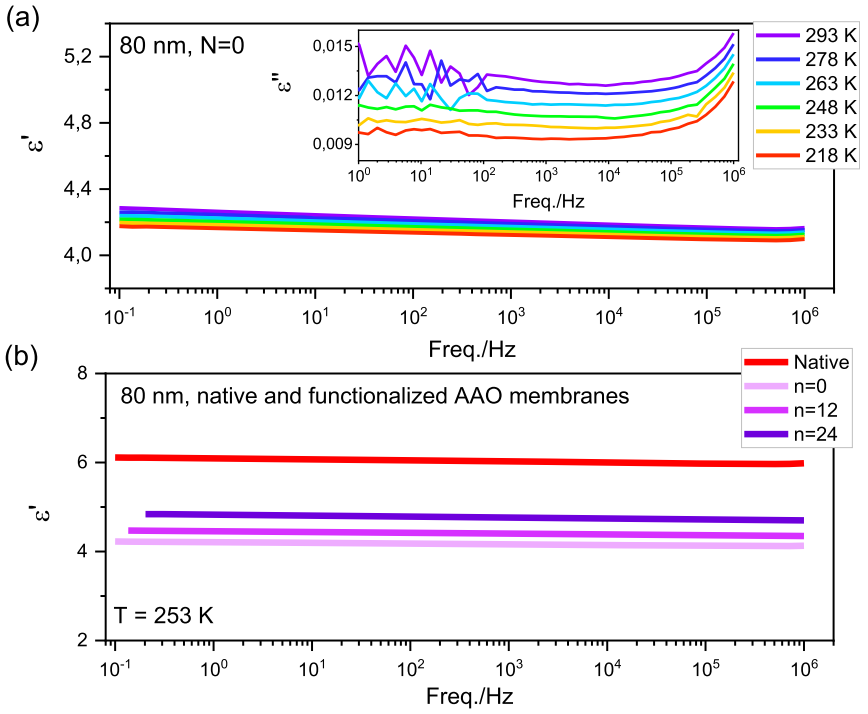

Figure 6. (a) Real and imaginary (inset) parts of the complex dielectric permittivity for the empty (air-filled) functionalized AAO membrane with $N = 0$ recorded on cooling from 293 to 218 K. The diameter of the nanopores is 80 nm. (b) Real part of the complex dielectric permittivity for the empty (air-filled) AAO membranes with pristine and chemically modified surface of the pore walls (from $N = 0$ to $N = 24$) as measured at 253 K.

temperature-independent for the functionalized alumina templates with $N = 0$ and can be considered loss-free (inset). In addition to that, native and modified AAO membranes with a pore diameter of 80 nm show frequency invariance of ε', as demonstrated in Figure 6b. The differences in the nature of the surface chemistry at the pore walls are reflected in the values of ε'. For native nanopores—rich with OH groups at the surface—the dielectric response of the empty membrane is higher compared to phosphonic acid-functionalized nanopores. Because empty membranes are filled with air ($\varepsilon'_{air} = 1$), finding the permittivity of the bare alumina matrix, ε_{AAO}, will also employ eq 2. The porosity of AAO membranes with 80 nm pore sizes is 13%, which makes $\varphi = 0.13$. In the next step, the correction of the dielectric data for PMPS 2.5k confined in such nanoporous templates was carried out accordingly with eq 2.

Figure 7 compares the pure polymer contribution with that of the polymer−matrix composite material. The representative dielectric loss curve for the tested polymer confined in native alumina nanopores is shifted toward higher values of ε'', as it depends only on the porosity of the membrane. The position of the maximum and the breadth of the α-loss peak remains the same. This is in line with the work by Alexandris and co-workers (see the Supporting Information therein), who also demonstrated that the only variable, which will be affected in such geometry is the absolute value of the dielectric permittivity.[56]

It should be noted that the scenario described above refers to the ideal situation when the nanopores are 100% filled with the investigated sample. However, in many cases, mainly due to high viscosity, the polymer imbibition within AAO nanopores is significantly impeded. In such a case, it is impossible to avoid air gaps inside the nanochannels, and additional corrections for some insulating blockage within the pore are needed. This can be done according to the procedure described in our recent paper.[69] If we assume that the nanopores are filled with PMPS 2.5k only up to 90%, we can also expect no shift of the α-peak, and spectral broadening (see Figure 7, "pure polymer, porosity, and air gap corrections").

Differential Scanning Calorimetry. Calorimetric measurements were carried out using a Mettler Toledo DSC apparatus equipped with a liquid nitrogen cooling accessory and an HSS8 ceramic sensor (heat flux sensor with 120 thermocouples). Temperature and

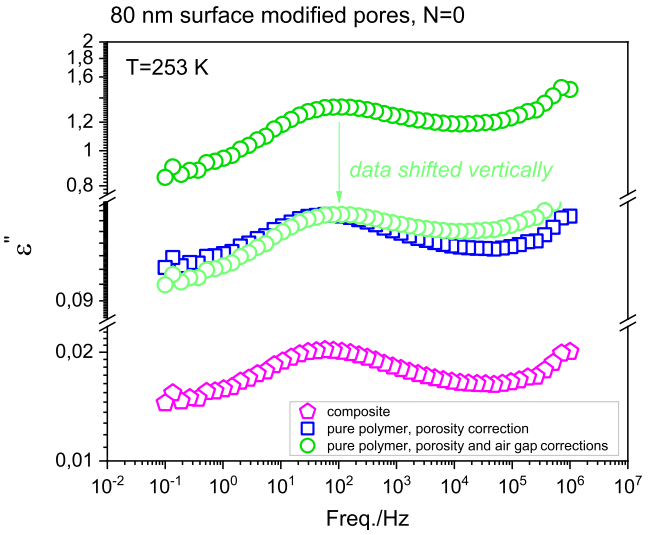

Figure 7. Dielectric loss spectrum for PMPS 2.5k embedded within AAO nanopores of 80 nm size with surface modified by phosphonic acid ($N = 0$), labeled as "composite". Data were recorded on subsequent cooling from 293 to 219 K with 0.2 K/min. The open blue squares are obtained by correcting the composite data by the porosity contribution (pure polymer and porosity correction). The green open circles are brought by including the correction for incomplete filling of the nanochannels with the polymer (up to 10%). All curves refer to 253 K.

enthalpy calibrations were performed by using indium and zinc standards. Crucibles with the prepared samples (bulk or either crushed alumina membranes containing confined PMPS) were sealed and cooled down to 183 K with the rate of either 0.5, 5, or 10 K/min inside a DSC apparatus. Then, DSC thermograms were recorded on heating with a rate of 10 K/min in the temperature range from 183 to 313 K. T_g values were determined from heat flow data as the point

https://doi.org/10.1021/acs.macromol.1c02145
Macromolecules XXXX, XXX, XXX−XXX

corresponding to the midpoint inflection of the extrapolated onset and end of the transition curve. The time-dependent measurements were also carried out using the same DSC system. Thermal protocol for such experiments involved:

1. Quench from T = 313 to T = 235 K.
2. Heating to T = 313 K upon which the DSC thermograms were collected.
3. Cooling to T = 247 K.
4. Waiting at 247 K for 10 h.

After annealing at 235 K, the sample was heated up to T = 313 K. Upon that heating run, we have recorded the DSC thermogram for the confined material. After annealing at 247 K, the sample was cooled down again to T = 183 K and then heated up while measuring heat flow changes continuously until it reaches T = 313 K. The heating and cooling rates were kept constant, 10 K/min.

RESULTS AND DISCUSSION

We start by demonstrating the difference in the surface properties after the functionalization of the alumina nanopores using highly polar propyl phosphoric acid units and the assumed number of nonpolar trimethoxysilane separators. All silanization steps were carefully described in the previous section. It should be noted that after such treatment, the surface properties of the alumina matrices are expected to change significantly. Therefore, the contact angle was measured. The literature data show that the pure AAO matrix shows hydrophilic properties.[70,71] In our results, the obtained value of the WCA for the native AAO nanopores is approximately 35°. This value decreases to 28° after 30 s after the dropping, possibly due to water getting inside the nanopores (see Figure 8). Interestingly, we have not observed

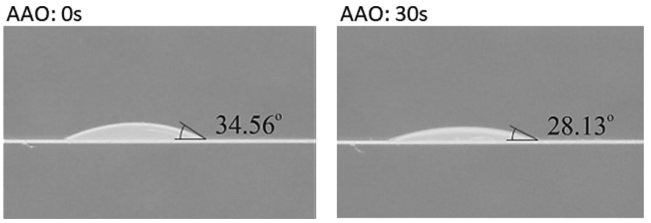

Figure 8. Results of contact-angle measurements for the reference sample: native AAO matrix.

this effect for functionalized samples. In this case, the contact angle remains unchanged in time. This proves that functionalization increases hydrophobicity in such a way that water is not able to penetrate pores in alumina oxide.

As we can see in Figure 9, most of the samples show a hydrophobic character[70] (contact angle of above 90°), except for the sample of AAO−$PO(OH)_2$−N0. However, this sample does not possess hydrophobic spacers but a relatively high concentration of dipolar phosphoric acid groups. The strongest hydrophobicity is observed for the sample AAO−$PO(OH)_2$−N24, according to our assumptions. In this case, we have 24 nonpolar spacer units per single polar phosphonic acid group. This material has the lowest dipolar character of the surface. With lowering the number of spacers per polar functional unit, we also observe increasing hydrophobicity of the surface. For the samples of AAO−$PO(OH)_2$−N12, AAO−$PO(OH)_2$−N6, and AAO−$PO(OH)_2$−N3, this increase is relatively low but constant. Much more significant changes are observed for the sample containing equimolar proportions of polar and nonpolar units [AAO−$PO(OH)_2$−N1], and the aforementioned sample of AAO−$PO(OH)_2$−N0. The dependency of the contact angle on the number of the spacer groups is shown in Figure 10. Based on these results, we conclude that

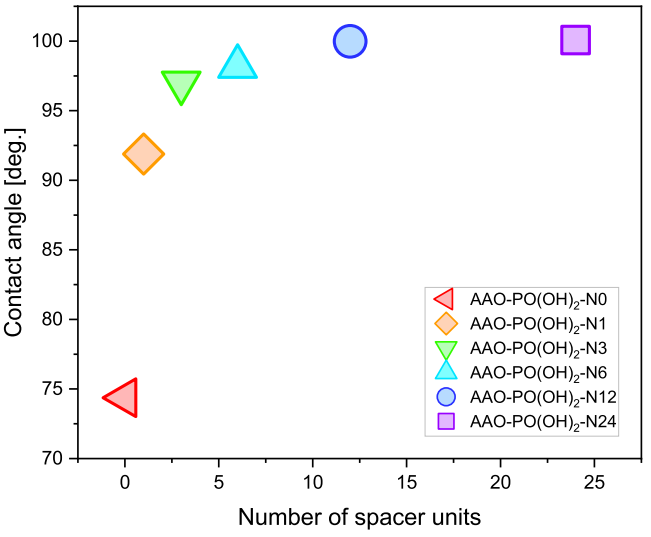

Figure 10. Dependency of the contact angle as a function of the number of the nonpolar spacer groups.

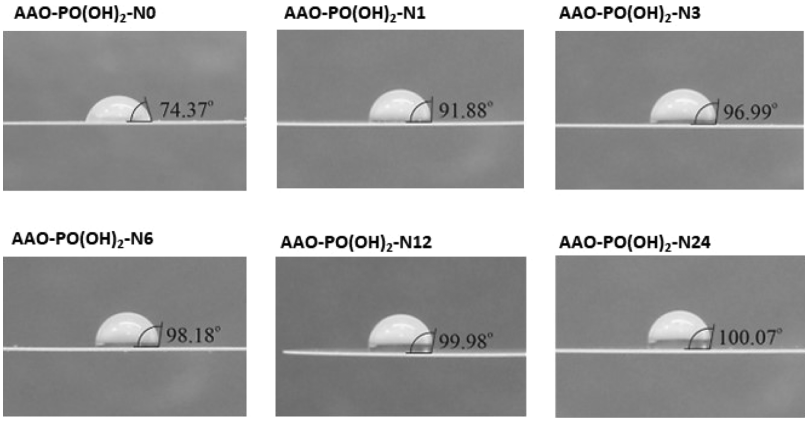

Figure 9. Results of contact-angle measurements for AAO nanoporous templates containing various concentrations of the polar phosphonic acid groups at the surface.

https://doi.org/10.1021/acs.macromol.1c02145
Macromolecules XXXX, XXX, XXX−XXX

with increasing N, the alumina nanopore properties are more hydrophobic. In the Supporting Information, we also provide measurements of WCA for the functionalized nonporous flat alumina surfaces and demonstrate that this trend is very similar.

Experimental evidence demonstrates that the hydrophobic and hydrophilic properties of the confining surfaces might significantly influence the glass-transition dynamics.[9,20,31,71] Therefore, in the next step, we have investigated changes in the segmental dynamics of the confined polymer induced by changing the surface polarity. From the previous work,[28,55] we know that in the dielectric spectra of bulk PMPS 2.5k one can detect three relaxation processes of different molecular origins: α', α, and β-relaxations. The former one is identified as the sub-Rouse mode, the second one is due to segmental mobility, and the latter one represents more local motions, though it is strongly coupled to the structural relaxation.

Figure 11 presents the dielectric loss spectra for the studied polymer confined within 80 nm-functionalized AAO nanopores measured at different temperatures, as indicated. In nanopore confinement, we found the two relaxation processes, α' and α. The slower one, α'-relaxation, is very broad and hardly noticeable due to its low intensity. Interestingly, when confined in AAO nanopores, the secondary β-relaxation is no longer observed. A similar finding we also reported for PMPS with higher molecular weight—27.7k (M_w)—confined in native AAO nanopores.[60] The lack of the β-relaxation under confinement was also seen in vapor-deposited glasses and epoxy resins constrained in alumina nanopores.[36,72] Such an effect might originate from the density variation or interactions with the constraining surface, which influences the geometry or induces conformational changes. As a consequence, the dipole moment libration of the molecule is affected too.

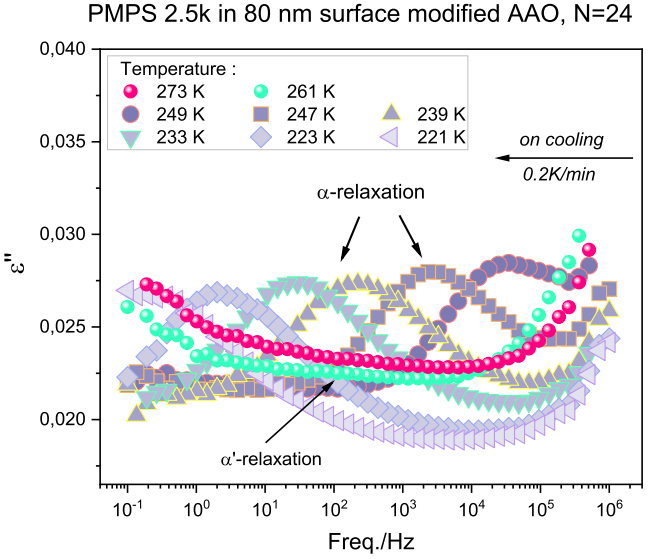

Figure 11. Dielectric loss spectra of PMPS 2.5k located in 80 nm AAO nanopores with functionalized pore walls (N = 24) as measured at different temperatures. The spectra shown are for the polymer–matrix composite material and were collected upon cooling with a rate of 0.2 K/min. Collected dielectric loss spectra were parameterized using the Havriliak–Negami (HN) function given as shown in ref.[73]

$$\varepsilon^*(\omega) = \varepsilon_\infty + \frac{\Delta\varepsilon}{[1 + (i\omega\tau_{HN})^a]^b} + \frac{\sigma_0}{i\omega\varepsilon_0} \quad (3)$$

where ε_∞ is the high-frequency limit of the permittivity, $\Delta\varepsilon$ is the dielectric strength, a and b are the shape parameters, σ_0 is the dc conductivity, τ_{HN} denotes the relaxation time, and ω is the angular frequency ($\omega = 2\pi f$). Using HN fitting parameters, the maximum of loss peak frequency f_{max} can be calculated from the following relation[74]

$$f_{max} = \frac{1}{\tau_{HN}}\left[\sin\left(\frac{a\pi}{2 + 2b}\right)\right]^{1/a}\left[\sin\left(\frac{ab\pi}{2 + 2b}\right)\right]^{-1/a} \quad (4)$$

The analysis of the collected dielectric loss spectra for α- and α'- processes performed from the fitting procedure has included the superposition of 2 HN functions. Finally, the relaxation times were obtained by calculating $\tau_{max} = 1/(2\pi f_{max})$. Because the intensity of the α'- peak in alumina nanopores is very low and the distribution of the relaxation time is very broad, the obtained $\tau_{\alpha'}(T)$ dependences were eliminated from subsequent consideration. We have only focused on the segmental dynamics of the studied polymer embedded within nanoporous templates with native and functionalized pore surfaces.

Figure 12a presents the temperature dependences of the α-relaxation time for PMPS 2.5k in the bulk and confined within AAO nanopores. The results were obtained upon heating with 0.2 K/min followed by rapid cooling with 10 K/min from 293 to 219 K. The segmental process for the bulk polymer exhibits Vogel–Fulcher–Tammann (VFT) behavior, therefore, can be approximated using the succeeding equation[75−77]

$$\tau_\alpha = \tau_\infty \exp\left(\frac{B}{T - T_0}\right) \quad (5)$$

where τ_∞ is the limiting relaxation time at very high temperatures, B is the activation parameter, while T_0 is the "ideal" glass temperature, often termed as a Vogel temperature. The results show that the segmental relaxation in phosphonic acid-functionalized nanopores with a varying number of nonpolar spacer groups attached to the pore walls follows bulk behavior at higher temperatures. However, as the temperature is decreased, we can observe some deviation from the bulk VFT dependence. These results coincide with our previous work on PMPS 2.5k confined in 55 nm size native and silanized AAO templates[28] as well as numerous literature works reported for other glass-forming substances in confined geometry.[17,40,78−81] Faster dynamics in nanopores compared to the bulk sample can be related, for example, with frustration in the density,[24,35,79] dynamic exchange between the surface layer and free molecules,[82] approaching the length scale of cooperative dynamics,[83] or crossing a spinodal temperature.[84]

In the next step, we have examined the effect of the different thermal protocols on the $\tau_\alpha(T)$ for the investigated polymer embedded within 80 nm treated and untreated AAO. In this case, the segmental relaxation times were measured upon (i) slow cooling from the room temperature with a rate of ∼0.2 K/min as well (ii) upon slow heating from the glassy state, which was followed by cooling with 10 K/min to low temperatures. The representative results for PMPS 2.5k in 80 nm native alumina pores are shown in Figure 12b. As can be seen, depending on the protocol $\tau_\alpha(T)$ evolves in a slightly different way. This indicates that the segmental relaxation of the studied polymer is in an out-of-equilibrium state. Notably, the same effect was also seen in nanoporous templates with varying surface polarity. In the temperature region, where the

https://doi.org/10.1021/acs.macromol.1c02145
Macromolecules XXXX, XXX, XXX−XXX

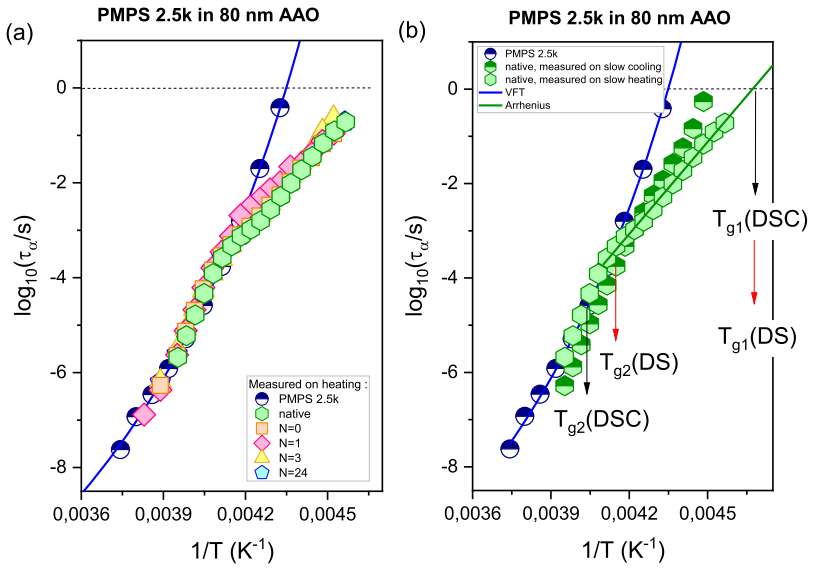

Figure 12. (a) Temperature dependence of the segmental relaxation times for PMPS 2.5k confined to 80 nm in diameter native and functionalized AAO nanopores with a varying number of nonpolar spacers per single polar phosphonic acid unit (from $N = 0$ to $N = 24$). The temperature dependence of the segmental relaxation time for the bulk polymer is shown as a reference. The data were measured on slow heating from lower temperatures; (b) $\tau_\alpha(T)$ for the tested polymer located in native alumina nanopores measured by following two different thermal protocols. Data were obtained either on cooling from higher temperatures or on heating from lower temperatures (followed by quench). The blue line is the VFT fit, while the green line represents Arrhenius fit to data. The T_g values for DSC and DS are also shown for reference.

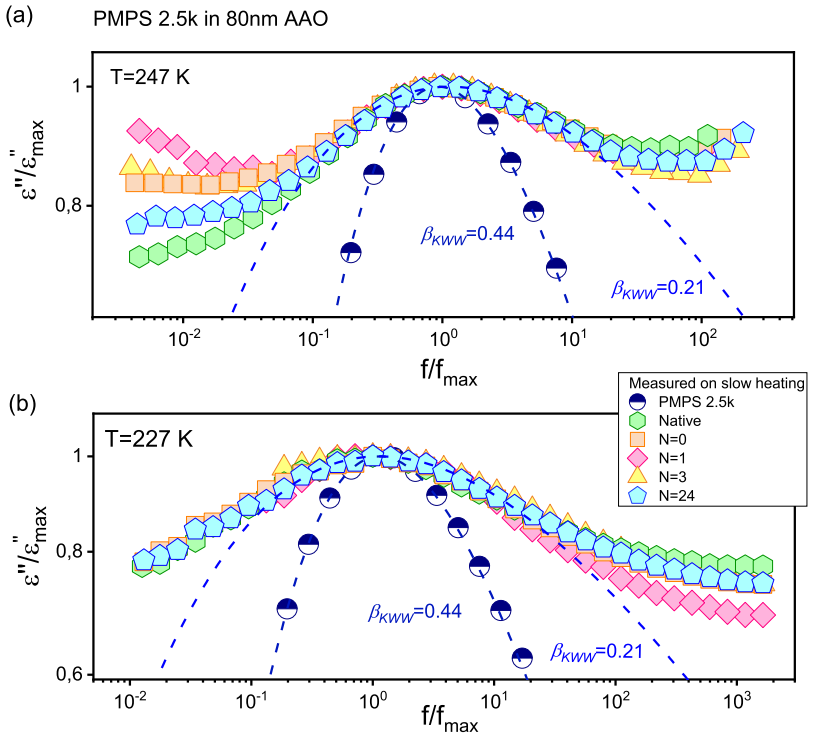

Figure 13. Comparison of the shape of the α-relaxation for PMPS 2.5k confined to native and surface-modified AAO nanopores with 80 nm pore sizes as measured on slow heating from the glassy state at two different temperatures, that is, (a) above and (b) below a characteristic kink in the $\tau_\alpha(T)$. Bulk spectra are given as a reference.

obtained dependences do not follow the VFT behavior anymore, we have approximated the evolution of τ_α using an Arrhenius equation[85]

$$\log \tau = \tau_\infty \exp\left(\frac{\Delta E}{k_B T}\right) \quad (6)$$

where ΔE is the activation energy and τ_∞ is a pre-exponential factor.

At this point, it is worth noting that the temperature at which the α-relaxation time starts to deviate from the bulk dependence (we labeled it in Figure 12b as T_{g2}) is often related to vitrification of the interfacial layer, that is, the fraction of molecules with retarded mobility due to interactions with the

https://doi.org/10.1021/acs.macromol.1c02145
Macromolecules XXXX, XXX, XXX−XXX

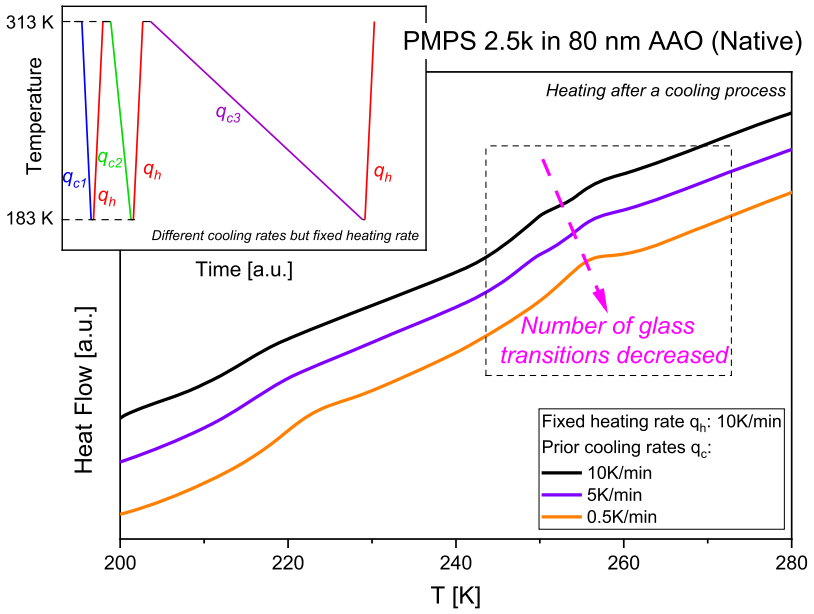

Figure 14. Standard DSC traces recorded for PMPS 2.5k located in 80 nm native AAO nanopores. The protocol of the measurement is shown in the inset. Samples were first cooled to 183 K and subsequently heated with a rate of 10 K/min.

pore walls.[19] Such a conclusion has been drawn by combining the results of the dielectric relaxation and calorimetric studies for some glass-forming systems confined in nanoporous alumina templates.[40,78] On the other hand, by extrapolating $\tau_\alpha(T)$ recorded at lower temperatures to 1 s, the glass-transition temperature of the remaining polymer chains in the core volume can be estimated. From that we get, T_{g1}(DS) = 213.5 K and T_{g2}(DS) = 241 K. By comparing the obtained results with that extracted from the calorimetric studies (shown in the further part of this paper), we found a very good agreement between T_{g1}(DS) and T_{g1}(DSC), which reflect vitrification within the core volume. However, a marked discrepancy was observed at higher temperatures, where the interfacial layer is expected to vitrify. We suppose that this might be related to the enormous sensitivity of the PMPS segmental dynamics to density frustration, which can be induced, for example, by changing even very slightly the thermal protocol.

We conclude this part by noting that for untreated alumina nanopores, the change in the segmental relaxation time is virtually the same as when we precisely control the polarity of the surface by adjusting the proportions between the polar functional units and nonpolar spacers. This is a very surprising result, especially that for PMPS 2.5k confined within 55 nm alumina templates with surface modified using either hydrophilic APTMOS or either more hydrophobic ClTMS, we could see a clear difference. In that case, the polymer dynamics confined within AAO membranes with the surface modified using APTMOS (contact angle value 28.16°) was faster compared to the bulk. While for the surfaces treated with ClTMS (the WCA ∼90°), we have not seen any deviation of $\tau_\alpha(T)$ from the bulk behavior.[28] Conversely, the confinement effect was clearly seen on DSC thermograms as the two distinct glass-transition events located above and below the vitrification temperatures of the bulk polymer were detected.

Apart from the analysis of the segmental relaxation times, it is also essential to compare the distribution of the α-relaxation time for native and phosphonic acid-functionalized nanopores with respect to the bulk polymer. We provide such comparison in Figure 13a,b. For the confined systems, the observed spectral broadening is widely reported in the literature. In addition, it indicates that the segmental relaxation becomes more heterogeneous in a spatially restricted environment.[17,74,86−88] As reported in the literature, by the silanization of the inner pore walls, the broadening of the α-relaxation peak in confinement might be even thoroughly eliminated.[17,21] However, the results presented in Figure 13a,b show no virtual difference in the breadth of the α-relaxation peak for PMPS 2.5k confined within treated and untreated nanoporous templates, neither at high nor at lower temperatures. The distribution of the α-relaxation time for all nanopore-confined samples is practically the same. It is evident that nanopore confinement itself is responsible for significantly broadening the relaxation time distribution. A particular surface condition plays here almost no role.

To describe more quantitatively the shape of the α-loss peak, we use the fractional exponent β_{KWW} from the Kohlrausch and Williams and Watts function[89,90]

$$\phi(t) = A \exp\left[-\left(\frac{t}{\tau}\right)^{\beta_{KWW}}\right] \quad (7)$$

where β_{KWW} varies from 0 to 1. It should be noted that the value of β_{KWW} decreases with increasing the width of the relaxation spectrum. The value of the stretching exponent obtained for PMPS 2.5k was confined in 80 nm alumina nanopores with varying surface polarity as measured at two different temperatures located above and below a characteristic kink in the $\tau_\alpha(T)$ dependence is 0.21, while for the bulk polymer, we get 0.44. By comparing the obtained values, we found a pronounced broadening of the α-loss peak in confined geometry, which—as mentioned before—is a typical sign of increasing heterogeneous relaxation dynamics in the presence of geometrical nanoconstraints. On the other hand, the change in the surface conditions from N = 0 to N = 24 practically does not affect the distribution of the α-relaxation times. At this point, we would like to recall our previous study on PMPS 2.5k confined within alumina templates with the surface of the

https://doi.org/10.1021/acs.macromol.1c02145
Macromolecules XXXX, XXX, XXX−XXX

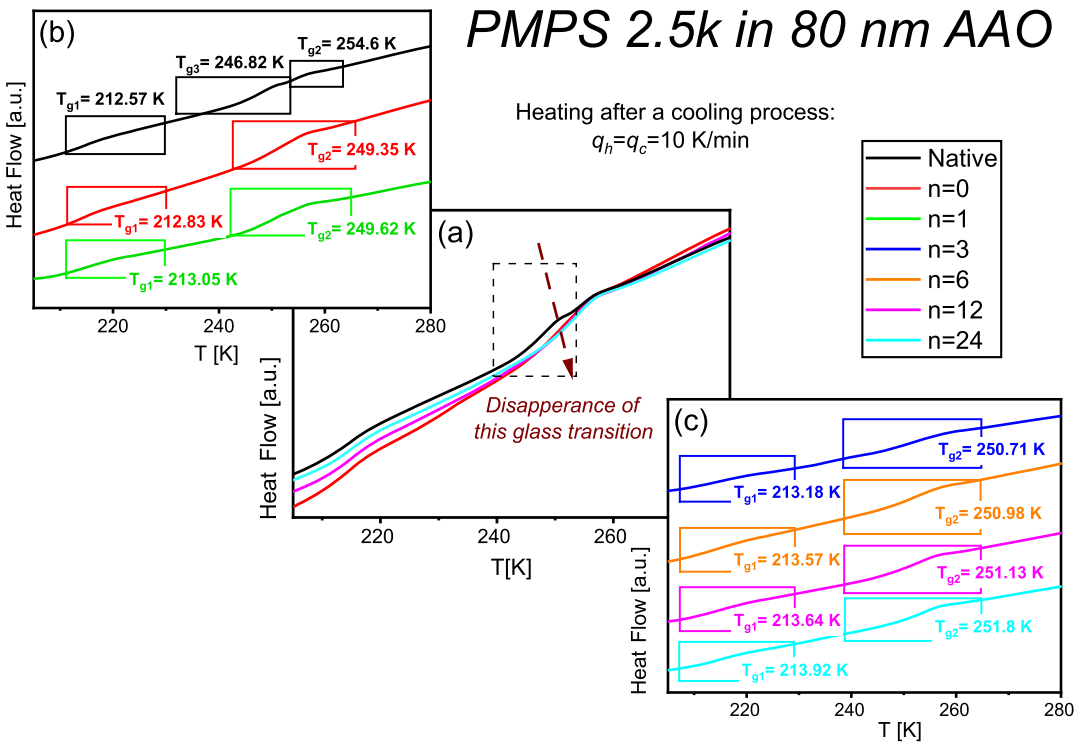

Figure 15. Standard DSC thermograms were recorded for PMPS 2.5k confined in AAO nanopores with the native and modified surfaces. Calorimetric data were recorded on heating with a rate of 10 K/min; after the previous cooling with 10 K/min. Panels (b,c) represent DSC curves in more detail, indicating the different T_g values for each case.

pores modified using different silanizing agents, ClTMS and APTMOS. The stretching exponents obtained for the ClTMS-treated pores was 0.36, while for a more hydrophilic APTMOS surface, we get 0.28.[28] Both values are larger compared to those reported in the present work. Based on that finding, we suppose that the breadth of the relaxation function, at least to some extent, senses changes in the chemical nature of the surface. However, the differences in the surface conditions induced by controlling the proportions between the polar functional units and nonpolar spacers do not make here any additional changes.

To confirm and verify the results derived from the dielectric measurements, we have also performed DSC for PMPS 2.5k confined in native and surface-modified nanopores. For this purpose, we have performed DSC scans using three different cooling rates: 10, 5, and 0.5 K/min, followed by heating with 10 K/min. The results collected in Figure 14 indicate that the number of glass-transition events for the native AAO nanopores decreases with decreasing the cooling rate. With the fastest cooling rate used in this study, that is, 10 K/min, we were able to observe three glass-transition events, while the intermediate and ultraslow cooling rates generate only two T_g's. This type of observation was reported for the first time by Li and co-workers for poly(methyl methacrylate) confined in alumina nanopores.[91] The origin of such a phenomenon was related to strong interfacial interactions between the polymer chains and the pore walls that can propagate into the center of the pore. As a result, an additional layer—so-called an interlayer—is formed. The interlayer is situated in between the core volume and adsorbed layer. Such a gradient in mobility results in three glass-transition events: T_{g1} (for the core volume), T_{g2} (for the interfacial), and T_{g3} (for the interlayer). The formation of each layer is a strongly nonequilibrium process; therefore, their thicknesses can change with time or the cooling rate in a different way.

Interestingly, as can be seen in Figure 15a–c, in DSC thermograms of the studied polymer confined in alumina nanopores with the modified surface polarity, we have not observed the presence of three T_g's. In contrast to native AAO nanopores, only two endothermic processes were detected in such cases. When changing the number of the nonpolar space units from N = 0 to N = 24, a small but systematic increase of T_{g1} and T_{g2} values is observed. Compared to native AAO nanopores, T_g values corresponding to the core volume are always slightly higher in silanized nanopores, while for the interfacial layer, they are lower. Herein, it is worth recalling our previous study on PMPS 2.5k confined in AAO nanopores with pore walls modified using ClTMS and APTMOS. In that case, we have also observed the presence of two glass-transition temperatures reflecting interfacial and core dynamics, while no calorimetric signatures of the interlayer formation. As we suppose, silanization of the surface walls cannot inhibit the formation of the adsorbed layer with frustrated dynamics. However, it effectively weakens the spread of the gradient in dynamics toward the center part of the pores.

Recent studies on polymer thin films and nanopore confinement highlight the important role of nonequilibrium phenomena in determining the behavior of confined glass-forming systems at the nanometer length scale.[31,35,38,40,42,80,92] In the presence of spatial restrictions comparable in size with the coil dimensions, the polymer chains cannot approach an equilibrium conformation within the time typically allowed for processing or stabilization of a new condition. As a result of the frustration in the density, deviations in segmental mobility is observed in a confined space. Nevertheless, when provided enough time, out-of-equilibrium chains can partially or

https://doi.org/10.1021/acs.macromol.1c02145
Macromolecules XXXX, XXX, XXX−XXX

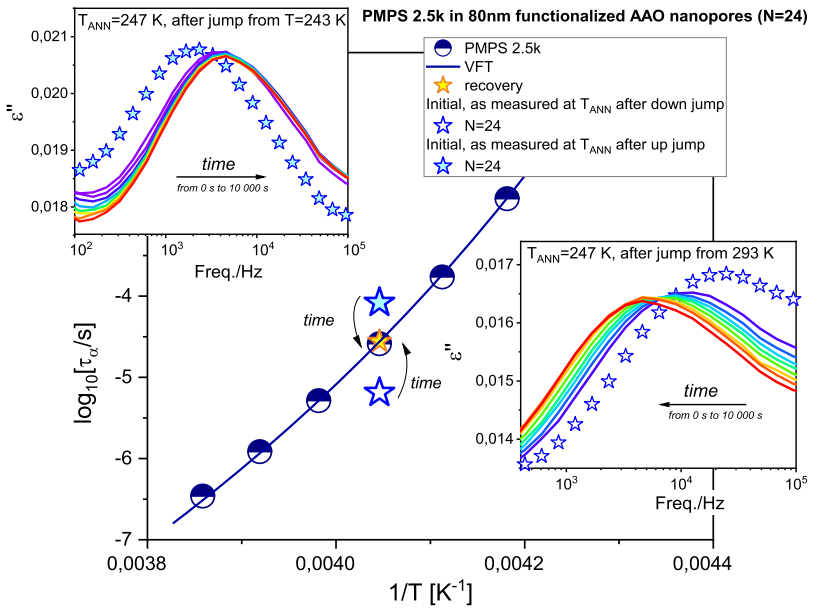

Figure 16. (main) Segmental relaxation times plotted vs the temperature for bulk PMPS 2.5k and confined to 80 nm surface-modified AAO nanopores (polar/nonpolar spacers, N = 24). The results were collected before ("initial") and after ("recovery") annealing at T_{ANN} = 247 K; previously, the samples experience two different thermal treatment protocols (up jump from 243 K and down jumps from 293 K). The solid line represents the fitting of the bulk data to the VFT equation. The upper and lower insets present changes in the α-loss peak position for the confined polymer at T_{ANN}.

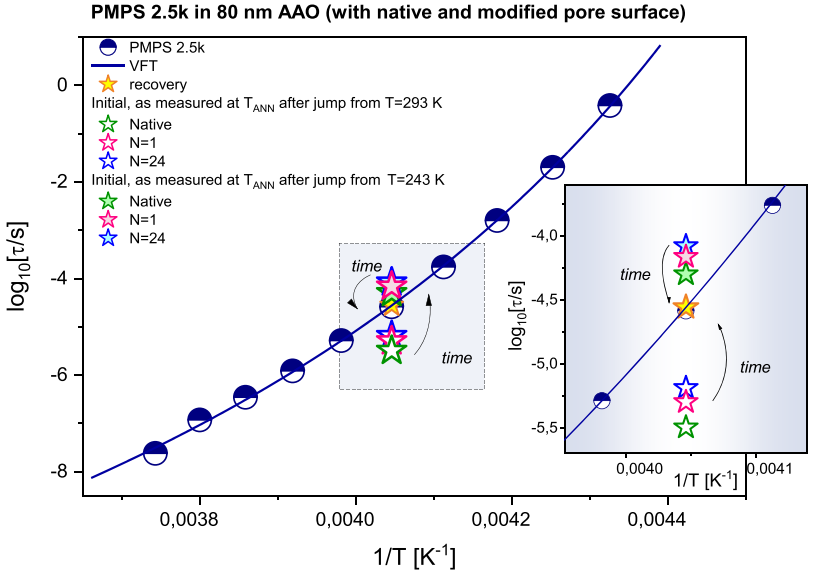

Figure 17. (main) Segmental relaxation times plotted vs the temperature for the bulk PMPS 2.5k and confined to 80 nm AAO nanopores with native and modified surfaces (polar/nonpolar spacers, N = 1 and N = 24). The results were collected before ("initial") and after ("recovery") annealing at T_{ANN} = 247 K; previously, the samples experience two different thermal treatment protocols (up jump from 243 K and down jumps from 293 K). The solid line represents the fitting of the bulk data to the VFT equation. Inset shows a close-up view of the data.

completely relax and approach an equilibrium configuration characteristic for a given state condition. This causes changes in the properties of the confined polymer with time.

Therefore, for the completeness of the present study, we wish to focus on nonequilibrium phenomena taking place in nanopore-confined geometry, and the role of surface chemistry in recovering the bulk-like behavior with time. For that purpose, we have carried out time-dependent dielectric and calorimetric measurements in the selected temperature conditions located just a few Kelvins below T_{g2} for a period of up to 20 h. Thermal protocol for such experiments involved quenches from the room temperature to a designated annealing temperature with or without an intermediate temperature jump. In the lower inset of Figure 16, we show representative time evolution of the dielectric loss spectra for the PMPS 2.5k confined in 80 nm AAO nanopores with 24 nonpolar group spacers at the surface after a jump in temperature from 293 K to T_{ANN} = 247 K. The shift of the α-loss peak toward lower frequencies with time indicates slowing down of the segmental dynamics. After waiting for a subsequent time at T_{ANN} = 247 K, the α-relaxation peak ceases to shift. Eventually, the confined polymer reaches the

https://doi.org/10.1021/acs.macromol.1c02145
Macromolecules XXXX, XXX, XXX−XXX

Table 1. Fitting Parameters from the Stretched Exponential Function Describing the Equilibration Kinetics of PMPS 2.5k Located in Native and Surface-Modified Alumina Templates with a Pore Diameter of 80 nm

parameters		sample					
		$N = 1$	$N = 3$	$N = 6$	$N = 12$	$N = 24$	native
T = 247 K after jump from T = 293 K	a	−0.82	−0.92	−0.84	−0.74	−0.70	−0.91
	b	−4.48	−4.37	−4.49	−4.54	−4.48	−4.59
	n	1.49	1.26	1.12	1.16	1.10	1.19
	$\log_{10}\tau_{ANN}$	3.04	3.17	3.21	3.24	3.29	3.21
T = 247 K after jump from T = 243 K	a	0.34	0.40	0.39	0.30	0.40	0.34
	b	−4.51	−4.46	−4.43	−4.50	−4.48	−4.65
	n	0.69	0.64	0.51	0.46	0.30	0.63
	$\log_{10}\tau_{ANN}$	2.57	2.43	2.39	2.23	2.01	2.40

relaxation time corresponding to the bulk sample (within 3−4 h of annealing). This recovery phenomenon we can follow by analyzing changes of the τ_α as a function of time. For clarity, in the main panel of Figure 16, we present the initial and final values of τ_α (noted as "down jump"). The same equilibration behavior was also seen in other cases. For both native and surface-modified nanopores, at a selected annealing temperature T_{ANN} = 247 K, it was possible to recover a τ_α characteristic for a bulk polymer, as shown in Figure 17. By looking closely at the initial values of the α-relaxation times measured at T_{ANN} = 247 K (inset in Figure 17), we found that for the samples that experience the same thermal protocol, the fastest dynamics is seen in native nanopores, while the slowest one in functionalized pores with the greater number of nonpolar spacer groups N = 24 (i.e., the most hydrophobic ones).

To analyze the equilibration kinetics in confined geometry, the evolution of the α-relaxation time upon annealing was described using a stretched exponential function given as

$$\tau_\alpha = a\cdot\exp(-t/\tau_{ANN})^n + b \quad (8)$$

where τ_{ANN} is a characteristic annealing time. The fitting parameters for confined polymer samples are collected in Table 1. The results indicate that for the down jump (from 293 to 247 K), the equilibration time increases with increasing the number of nonpolar group spacers attached to the pore surface.

Apart from doing a down jump from the equilibrium state of faster dynamics (293 K) to the nonequilibrium state of slower dynamics (247 K), we have also carried out time-dependent measurements at the selected annealing temperatures T_{ANN} = 247 K in the up-jump conditions. To do that, the tested samples were first cooled down from room temperature to a pre-initial annealing temperature, T_{ANN} 5K = 243 K. At this temperature, the sample was allowed to completely recover so that the τ_α approach the value characteristic for a bulk polymer at a given temperature. Only after that, an up jump in temperature was performed from 243 to 247 K. The upper inset in Figure 16 demonstrates the corresponding changes in the dielectric loss spectra recorded for PMPS 2.5k confined in silanized nanopores (N = 24) upon the equilibration process at T_{ANN} for such cases. In contrast to the down-jump conditions, the segmental mobility is reduced compared to the bulk, but it progressively increases with time. The peak maximum shifts toward higher frequencies and eventually reaches the same relaxation time as for the bulk (it takes ∼2 h). Although the depths of the up and down jumps are not the same (ΔT for down > up), we can still extract some interesting information regarding equilibration phenomena in a nanopore confinement. A close study of the inset in Figure 17 reveals that the initial values of the α-relaxation times, measured at T_{ANN} = 247 K immediately after an up jump, follow a completely different trend than that seen for down-jump conditions. Initially, the segmental mobility of the confined PMPS is the slowest in AAO nanopores with N = 24 nonpolar spacer groups per single polar unit, while its the fastest in native nanopores. The analysis of the equilibration kinetics with the use of the stretched exponential function also reveals a very interesting finding. Namely, with increasing the number of nonpolar spacer groups at the pore surface, the confined polymer recovers toward equilibrium faster. Table 1 lists the parameters obtained from the analysis of the $\tau_\alpha(t)$ with the use of a stretched exponent. For better visualization, in Figure 18, we also summarize the behavior of the characteristic annealing times as a function of the ratio between the polar and nonpolar units. In the case of up jumps, the hydrophobic surface conditions facilitate recovery in confinement, while for the down jumps—they are not favorable. From that, we presume that by changing precisely the surface polarity, it is possible to control the time of the structural recovery toward the equilibrium state.

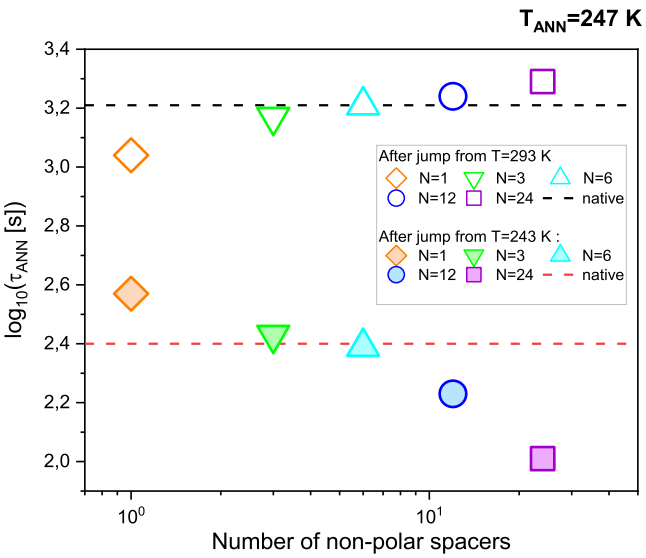

Figure 18. Dependence of the annealing time for the different ratio values between polar and nonpolar units used for surface modification of AAO nanopores. Dashed lines represent annealing time constants for native nanopores.

In line with the dielectric measurements, we have also performed annealing experiments using DSC. The two tested

https://doi.org/10.1021/acs.macromol.1c02145
Macromolecules XXXX, XXX, XXX−XXX

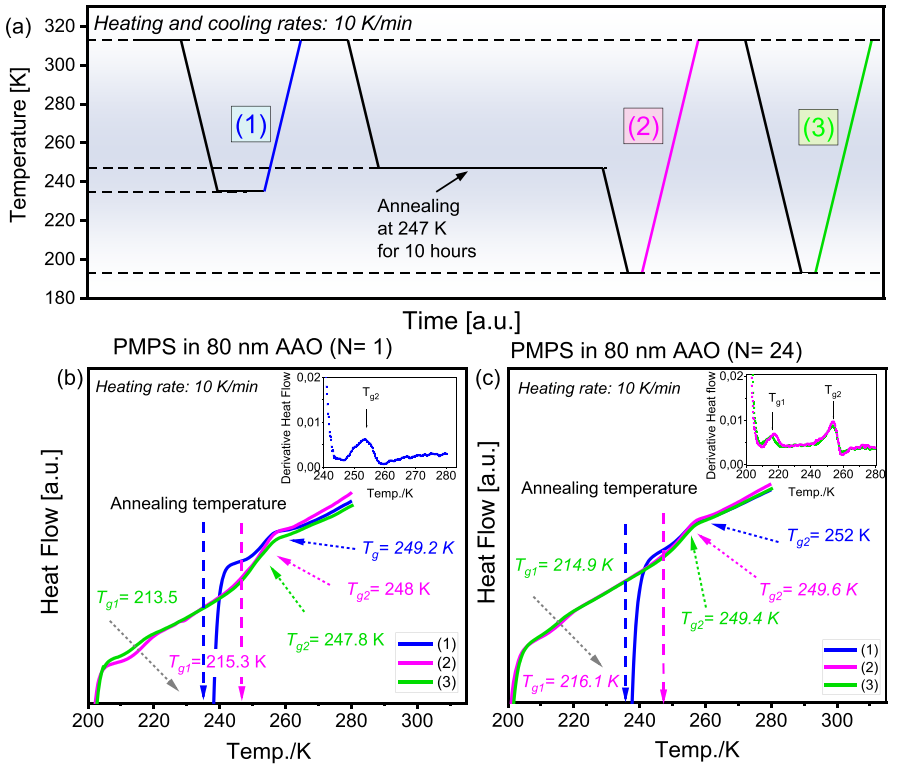

Figure 19. (a) DSC protocol used for PMPS 2.5k in 80 nm AAO templates with the varying pore surface polarity, N = 1 and N = 24. Curves (1) were recorded on the heating from T = 235 to T = 313 K, after annealing at T = 235 K; curves (2) were collected on the heating from T = 183 to T = 313 K after prior annealing at T = 247 K for 10 h; curves (3) refer to the measurements on the heating from T = 183 to T = 313 K without any prior annealing. Panels (b,c) show DSC thermograms (and heat flow derivatives) indicating different T_g values for N = 1 and N = 24, respectively. DSC data were recorded on heating with a rate of 10 K/min, following cooling with 10 K/min.

samples were PMPS 2.5k confined in AAO nanopores with modified surface polarity, N = 1 and N = 24. Figure 19a illustrates the detailed steps of the experimental procedure. Politidis et al. reported that without crossing the low T_{g1} the higher T_{g2} does not appear on DSC scans for *cis*-1,4-polyisoprene confined in AAO nanopores.[84] Keeping that in mind, we first aim to test if T_{g2} can be detected on DSC traces of the studied confined systems when T_{g1} is not crossed. The annealing temperature T = 235 K matches these requirement conditions. Therefore, after cooling from 313 to 235 K ($T_{g1} < T < T_{g2}$), the samples were isothermally annealed for 2 h. Then, the heating scan was performed from 235 to 313 K (without cooling to lower temperatures). The results, as shown in Figure 19b,c (blue lines), demonstrate the presence of T_{g2} in calorimetric data, though we have not cooled down the sample to lower temperatures, that is, below T_{g1}. From that, we see that the appearance of T_{g2} is not conditional concerning crossing T_{g1}. Interestingly, the same conclusion was also made for PMPS with a higher molecular weight (21.7k) confined within 100 nm AAO nanopores. The results of the calorimetric studies, which are presented in the Supporting Information, demonstrate that the presence of high T_{g2} does not depend on the molecular weight, in contrast to *cis*-1,4 PI studied by Floudas and co-workers.[84] In the next run, isothermal annealing was performed at T_{ANN} = 247 K for 10 h. After a given annealing time, the sample was cooled down to 183 K and then measured upon subsequent heating (i.e., upon crossing the temperature region at which T_{g1} is observed). Lastly, the sample was cooled to 183 K with 10 K/min and reheated at the same rate, while omitting the annealing step. Figure 19b,c shows the obtained results for the tested polymer confined in AAO nanopores with the two limiting surface polarity conditions, N = 1 and N = 24, respectively. The first important information extracted from the thermograms is that prolonged annealing carried out at 247 K does not clear out completely the confinement effects on heating. More specifically, even if the equilibrium state is regained in the previous step, subsequent cooling of the sample to lower temperatures drives it out of the equilibrium again. The equilibration phenomenon is, however, seen in the values of T_{g1} and T_{g2}. After prolonged annealing at 247 K, T_{g1} shifts toward higher temperatures, while T_{g2} toward lower temperatures, when compared to the freshly prepared (not-annealed) samples.

It is still not entirely clear why the two T_g scenarios are sometimes seen for the nanopore-confined samples. We have detected it in all of the cases, though the inner surface of the pores was modified via different strategies, including changes in the polarity and hydrophobicity/hydrophilicity. This suggests that the presence of T_{g2} does not depend strongly on the surface chemistry. The modification of the surface conditions aims to affect the specific interactions of the polymer with the confining walls causing T_{g2} to disappear. However, the presence of two T_g's has also been seen even in the absence of strong interactions for other systems.[93] One of the possibilities, noted by Wang et al., is to link high and low T_g's seen in nanopore confinement with a variation in the density, which for the regions close to the smooth pores induce denser packing, while for the regions away from the pores results in consistently lower density areas.[93] Such an

https://doi.org/10.1021/acs.macromol.1c02145
Macromolecules XXXX, XXX, XXX−XXX

explanation would explain the disappearance of two T_g scenarios for rough pore walls.[94] What the current study shows is that the particular surface chemistry can either promote or hinder the equilibration phenomena that bring back the nanoconfined system to the time scale of the bulk material.

It should be noted that except for the particular changes in the surface conditions, like that induced by controlling the number of nonpolar spacer groups attached to the nanopore walls, the interfacial energy is expected to play a significant role in controlling segmental dynamics of the polymer under nanopore confinement. This was demonstrated for polymer materials by Alexandris et al.[56] as well as for the low-molecular compounds by Talik et al.[25] Typically, with increasing the interfacial energy between the polymer and the alumina surface, the glass-transition temperature of the core fraction is decreased compared to the bulk material. On the other hand, as interfacial energy increases, the glass-transition temperature of the interfacial layer was found to increase. By knowing that this is a general trend observed for numerous polymers and molecular systems in confined geometry, we have determined the surface and interface properties of PMPS 2.5k and alumina substrates (native and modified). The details of such calculation can be found in the Supporting Information. The results presented in Figure 20, demonstrate that with

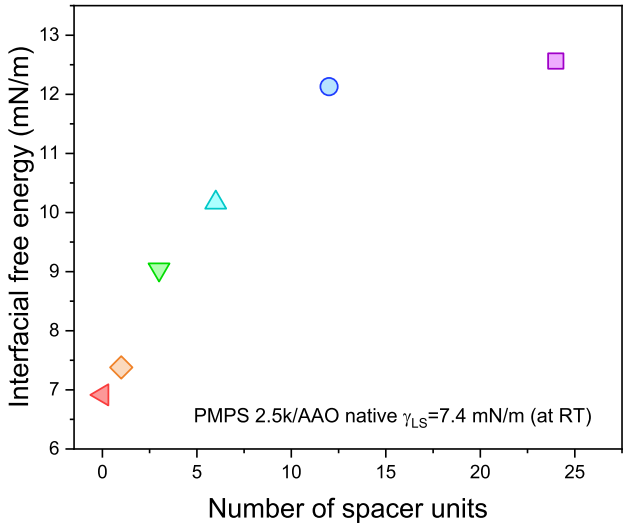

Figure 20. Dependency of the interfacial free energy γ_{SL} for PMPS 2.5k/alumina substrates as a function of the number of the nonpolar spacer groups attached to the surface. Based on contact-angle measurements performed at room temperature.

increasing the number of nonpolar spacers at the alumina surface (from $N = 0$ to $N = 24$), the interfacial energy between PMPS and the considered confining substrates increases, from ~7.4 to 12.5 mN/m. This suggests stronger interactions of the polymer with the substrate with increasing number of nonpolar spacer units attached to the alumina surface. In contrast to that, when changing the number of the nonpolar space units from $N = 0$ to $N = 24$, the differences in the values of the glass-transition temperatures recorded for core and interfacial fractions are only within few Kelvins (DSC data shown in Figure 15). Both systematically increase, but still the observed differences are very subtle. By combining these two findings, we can conjecture that, for the series of the investigated PMPS samples confined in AAO templates with modulated surface polarity, the changes in the interfacial energy do not produce well-pronounced differences in T_g values for the core and interfacial layers. However, it does not mean that the interfacial energy between PMPS and alumina templates with either native or modified pore walls is insignificant. As a matter of fact, it should have a substantial effect on the confined polymer dynamics. We can expect that by taking into account a large downward shift of the glass-transition temperature in confined geometry, that is, $\Delta T_g = T_{gcore} - T_{g,bulk}$, which for the tested polymer is approx. within (−16) to (−18) K. Based on the literature data, the estimated value of the interfacial energy for PMPS with similar $M_n \sim 2200$ g/mol confined in native AAO templates is 7.4 mN/m.[56] In contrast, almost no shift in T_g is observed for glycerol with extremely low interfacial energy, γ_{SL} = 1.5 mN/m.[25]

CONCLUSIONS

In this work, by employing DS and DSC, we have investigated the influence of the changes in surface polarity on the segmental dynamics of PMPS 2.5k confined in nanoporous alumina templates with 80 nm pore diameter. To control the surface conditions, we have functionalized AAO membranes using highly polar propyl phosphoric units separated by the assumed concentration on nonpolar triethoxysilane groups. By adjusting the proportions between polar functional units and nonpolar spacers (from $N = 0$ to $N = 24$), it was possible to control the polarity of the surface and, therefore, also the hydrophobic character of the pore walls. Induced in this way, changes in the surface conditions turned out to affect various aspects of the confined polymer dynamics. The most significant ones include reducing the gradient in mobility that propagates from polymer chains strongly bound to the pore walls into the center of the pores. Chemical modification of the surface prevents the formation of the interlayer located between the interfacial layer and the core volume. The interlayer is seen as an additional glass-transition event on DSC thermograms of the nanopore-confined polymer. Calorimetric results also indicate that in none of the studied samples, the modification of the surface conditions inhibits the formation of the adsorbed layer. Therefore, upon cooling, we a deviation of $\tau_\alpha(T)$ from the bulk behavior is observed. With increasing the number of nonpolar spacer groups attached to the pore walls, the glass-transition temperatures assigned to the adsorbed layer and core volume progressively shift toward higher temperatures. As these changes are very subtle (only within a few Kelvins), they cannot be seen clearly in $\tau_\alpha(T)$ for the confined polymer. Because in the temperature region located below the glass-transition temperature of the interfacial layer, the confined polymer is in an out-of-equilibrium state, we were able to study the structural recovery. The bulk-like evolution of the segmental relaxation time can be restored by prolonged annealing. Interestingly, we found that the changes in the surface polarity affect the equilibration kinetics and can be used to control the time of the structural recovery toward the equilibrium state. In the case of the functionalized nanopores with increasing the number of nonpolar spacer units per single polar group, the recovery from the confinement effect is favored for up-jump conditions, while retarded when doing down temperature jumps. This study also shows that the breadth of the relaxation function is an important parameter that can sense differences in the surface conditions. In confined geometry, we typically observe a pronounced broadening of the α-loss peak that can be itself affected just by

https://doi.org/10.1021/acs.macromol.1c02145
Macromolecules XXXX, XXX, XXX−XXX

changing the functionalization strategy. In this picture, our result sheds new light on the role of the surface conditions on the glass-transition dynamics of the nanopore-confined polymers, specifically, knowing that the behavior of nanopore-confined systems are strongly affected by various factors, such as thermal treatment, surface chemistry, or interfacial interactions. Understanding their individual role and complex interrelation will help design polymer nanomaterials with controlled physical properties and stability required for many applications.

■ ASSOCIATED CONTENT

Supporting Information

The Supporting Information is available free of charge at https://pubs.acs.org/doi/10.1021/acs.macromol.1c02145.

Results of calorimetric studies for PMPS 21.k, water contact-angle measurements made on flat nonporous alumina, characterization of the obtained samples and verification of each step of the surface modification strategy, and calculation of the surface and interfacial properties of PMPS 2.5k and flat alumina substrates (native and modified) (PDF)

■ AUTHOR INFORMATION

Corresponding Authors

Roksana Winkler − *Institute of Physics, University of Silesia, Chorzow 41-500, Poland; Silesian Center for Education and Interdisciplinary Research (SMCEBI), Chorzow 41-500, Poland;* orcid.org/0000-0001-8713-4308; Email: rwinker@us.edu.pl

Karolina Adrjanowicz − *Institute of Physics, University of Silesia, Chorzow 41-500, Poland; Silesian Center for Education and Interdisciplinary Research (SMCEBI), Chorzow 41-500, Poland;* orcid.org/0000-0003-0212-5010; Email: kadrjano@us.edu.pl

Authors

Wenkang Tu − *Institute of Physics, University of Silesia, Chorzow 41-500, Poland; Silesian Center for Education and Interdisciplinary Research (SMCEBI), Chorzow 41-500, Poland;* orcid.org/0000-0001-8895-4666

Mateusz Dulski − *Silesian Center for Education and Interdisciplinary Research (SMCEBI), Chorzow 41-500, Poland; Institute of Materials Engineering, University of Silesia, Chorzow 41-500, Poland;* orcid.org/0000-0001-8686-1853

Lukasz Laskowski − *Institute of Nuclear Physics Polish Academy of Sciences, Krakow 31-342, Poland*

Complete contact information is available at: https://pubs.acs.org/10.1021/acs.macromol.1c02145

Notes

The authors declare no competing financial interest.

■ ACKNOWLEDGMENTS

This work has been supported by the resources of the National Science Centre [grant-no: 2017/27/B/ST3/00402 (K.A.) and 2017/26/E/ST5/00162 (Ł.L.)].

■ REFERENCES

(1) García-Gutiérrez, M.-C.; Linares, A.; Hernández, J. J.; Rueda, D. R.; Ezquerra, T. A.; Poza, P.; Davies, R. J. Confinement-Induced One-Dimensional Ferroelectric Polymer Arrays. *Nano Lett.* **2010**, *10*, 1472−1476.

(2) Ghosh, S.; Kouamé, N. A.; Ramos, L.; Remita, S.; Dazzi, A.; Deniset-Besseau, A.; Beaunier, P.; Goubard, F.; Aubert, P.-H.; Remita, H. Conducting Polymer Nanostructures for Photocatalysis under Visible Light. *Nat. Mater.* **2015**, *14*, 505−511.

(3) Cho, J.; Hong, J.; Char, K.; Caruso, F. Nanoporous Block Copolymer Micelle/Micelle Multilayer Films with Dual Optical Properties. *J. Am. Chem. Soc.* **2006**, *128*, 9935−9942.

(4) Nejati, S.; Lau, K. K. S. Pore Filling of Nanostructured Electrodes in Dye Sensitized Solar Cells by Initiated Chemical Vapor Deposition. *Nano Lett.* **2011**, *11*, 419−423.

(5) Yang, X.; Loos, J.; Veenstra, S. C.; Verhees, W. J. H.; Wienk, M. M.; Kroon, J. M.; Michels, M. A. J.; Janssen, R. A. J. Nanoscale Morphology of High-Performance Polymer Solar Cells. *Nano Lett.* **2005**, *5*, 579−583.

(6) Richert, R. Dynamics of Nanoconfined Supercooled Liquids. *Annu. Rev. Phys. Chem.* **2011**, *62*, 65−84.

(7) Alcoutlabi, M.; McKenna, G. B. Effects of Confinement on Material Behaviour at the Nanometre Size Scale. *J. Phys.: Condens. Matter* **2005**, *17*, R461−R524.

(8) Jackson, C. L.; McKenna, G. B. Vitrification and Crystallization of Organic Liquids Confined to Nanoscale Pores. *Chem. Mater.* **1996**, *8*, 2128−2137.

(9) Kremer, F. *Dynamics in Geometrical Confinement*; Springer: Cham, 2014.

(10) Park, J.-Y.; McKenna, G. B. Size and Confinement Effects on the Glass Transition Behavior of Polystyrene/ o -Terphenyl Polymer Solutions. *Phys. Rev. B: Condens. Matter Mater. Phys.* **2000**, *61*, 6667−6676.

(11) Kremer, F.; Huwe, A.; Schönhals, A.; Różański, S. A. Molecular Dynamics in Confining Space. In *Broadband Dielectric Spectroscopy*; Springer Berlin Heidelberg: Berlin, Heidelberg, 2003; pp 171−224. DOI: 10.1007/978-3-642-56120-7_6

(12) Frank, B.; Gast, A. P.; Russell, T. P.; Brown, H. R.; Hawker, C. Polymer Mobility in Thin Films. *Macromolecules* **1996**, *29*, 6531−6534.

(13) Ediger, M. D.; Forrest, J. A. Dynamics near Free Surfaces and the Glass Transition in Thin Polymer Films: A View to the Future. *Macromolecules* **2014**, *47*, 471−478.

(14) Reiter, G. Dewetting as a Probe of Polymer Mobility in Thin Films. *Macromolecules* **1994**, *27*, 3046−3052.

(15) Li, Y.; Wei, D.; Han, C. C.; Liao, Q. Dynamics of Polymer Melts Confined by Smooth Walls: Crossover from Nonentangled Region to Entangled Region. *J. Chem. Phys.* **2007**, *126*, 204907.

(16) Keddie, J. L.; Jones, R. A. L.; Cory, R. A. Size-Dependent Depression of the Glass Transition Temperature in Polymer Films. *Europhys. Lett.* **1994**, *27*, 59−64.

(17) Arndt, M.; Stannarius, R.; Gorbatschow, W.; Kremer, F. Dielectric Investigations of the Dynamic Glass Transition in Nanopores. *Phys. Rev. E* **1996**, *54*, 5377−5390.

(18) Zhang, J.; Liu, G.; Jonas, J. Effects of Confinement on the Glass Transition Temperature of Molecular Liquids. *J. Phys. Chem.* **1992**, *96*, 3478−3480.

(19) Li, L.; Zhou, D.; Huang, D.; Xue, G. Double Glass Transition Temperatures of Poly(Methyl Methacrylate) Confined in Alumina Nanotube Templates. *Macromolecules* **2014**, *47*, 297−303.

(20) Reid, D. K.; Alves Freire, M.; Yao, H.; Sue, H.-J.; Lutkenhaus, J. L. The Effect of Surface Chemistry on the Glass Transition of Polycarbonate Inside Cylindrical Nanopores. *ACS Macro Lett.* **2015**, *4*, 151−154.

(21) Kipnusu, W. K.; Elmahdy, M. M.; Elsayed, M.; Krause-Rehberg, R.; Kremer, F. Counterbalance between Surface and Confinement Effects As Studied for Amino-Terminated Poly(Propylene Glycol) Constraint in Silica Nanopores. *Macromolecules* **2019**, *52*, 1864−1873.

(22) Zhang, C.; Li, L.; Wang, X.; Xue, G. Stabilization of Poly(Methyl Methacrylate) Nanofibers with Core−Shell Structures Confined in AAO Templates by the Balance between Geometric

Curvature, Interfacial Interactions, and Cooling Rate. *Macromolecules* **2017**, *50*, 1599−1609.
(23) Iacob, C.; Runt, J. Charge Transport of Polyester Ether Ionomers in Unidirectional Silica Nanopores. *ACS Macro Lett.* **2016**, *5*, 476−480.
(24) Kipnusu, W. K.; Elsayed, M.; Kossack, W.; Pawlus, S.; Adrjanowicz, K.; Tress, M.; Mapesa, E. U.; Krause-Rehberg, R.; Kaminski, K.; Kremer, F. Confinement for More Space: A Larger Free Volume and Enhanced Glassy Dynamics of 2-Ethyl-1-Hexanol in Nanopores. *J. Phys. Chem. Lett.* **2015**, *6*, 3708−3712.
(25) Talik, A.; Tarnacka, M.; Geppert-Rybczynska, M.; Minecka, A.; Kaminska, E.; Kaminski, K.; Paluch, M. Impact of the Interfacial Energy and Density Fluctuations on the Shift of the Glass-Transition Temperature of Liquids Confined in Pores. *J. Phys. Chem. C* **2019**, *123*, 5549−5556.
(26) Schönhals, A.; Goering, H.; Schick, C.; Frick, B.; Zorn, R. Glass Transition of Polymers Confined to Nanoporous Glasses. *Colloid Polym. Sci.* **2004**, *282*, 882−891.
(27) Kipnusu, W. K.; Elsayed, M.; Krause−Rehberg, R.; Kremer, F. Glassy Dynamics of Polymethylphenylsiloxane in One- and Two-Dimensional Nanometric Confinement—A Comparison. *J. Chem. Phys.* **2017**, *146*, 203302.
(28) Winkler, R.; Tu, W.; Laskowski, L.; Adrjanowicz, K. Effect of Surface Chemistry on the Glass-Transition Dynamics of Poly(Phenyl Methyl Siloxane) Confined in Alumina Nanopores. *Langmuir* **2020**, *36*, 7553−7565.
(29) Gainaru, C.; Schildmann, S.; Böhmer, R. Surface and Confinement Effects on the Dielectric Relaxation of a Monohydroxy Alcohol. *J. Chem. Phys.* **2011**, *135*, 174510.
(30) Brás, A. R.; Dionísio, M.; Schönhals, A. Confinement and Surface Effects on the Molecular Dynamics of a Nematic Mixture Investigated by Dielectric Relaxation Spectroscopy. *J. Phys. Chem. B* **2008**, *112*, 8227−8235.
(31) Chat, K.; Tu, W.; Laskowski, L.; Adrjanowicz, K. Effect of Surface Modification on the Glass Transition Dynamics of Highly Polar Molecular Liquid S-Methoxy-PC Confined in Anodic Aluminum Oxide Nanopores. *J. Phys. Chem. C* **2019**, *123*, 13365−13376.
(32) Iacob, C.; Sangoro, J. R.; Papadopoulos, P.; Schubert, T.; Naumov, S.; Valiullin, R.; Kärger, J.; Kremer, F. Charge Transport and Diffusion of Ionic Liquids in Nanoporous Silica Membranes. *Phys. Chem. Chem. Phys.* **2010**, *12*, 13798−13803.
(33) Li, M.; Wu, H.; Huang, Y.; Su, Z. Effects of Temperature and Template Surface on Crystallization of Syndiotactic Polystyrene in Cylindrical Nanopores. *Macromolecules* **2012**, *45*, 5196−5200.
(34) Napolitano, S. *Non-Equilibrium Phenomena in Confined Soft Matter: Irreversible Adsorption, Physical Aging and Glass Transition at the Nanoscale*; Springer, 2015.
(35) Adrjanowicz, K.; Paluch, M. Discharge of the Nanopore Confinement Effect on the Glass Transition Dynamics via Viscous Flow. *Phys. Rev. Lett.* **2019**, *122*, 176101.
(36) Tarnacka, M.; Dulski, M.; Geppert-Rybczyńska, M.; Talik, A.; Kamińska, E.; Kamiński, K.; Paluch, M. Variation in the Molecular Dynamics of DGEBA Confined within AAO Templates above and below the Glass-Transition Temperature. *J. Phys. Chem. C* **2018**, *122*, 28033−28044.
(37) Tarnacka, M.; Kaminski, K.; Mapesa, E. U.; Kaminska, E.; Paluch, M. Studies on the Temperature and Time Induced Variation in the Segmental and Chain Dynamics in Poly(Propylene Glycol) Confined at the Nanoscale. *Macromolecules* **2016**, *49*, 6678−6686.
(38) Tarnacka, M.; Madejczyk, O.; Kaminski, K.; Paluch, M. Time and Temperature as Key Parameters Controlling Dynamics and Properties of Spatially Restricted Polymers. *Macromolecules* **2017**, *50*, 5188−5193.
(39) Tarnacka, M.; Kaminska, E.; Kaminski, K.; Roland, C. M.; Paluch, M. Interplay between Core and Interfacial Mobility and Its Impact on the Measured Glass Transition: Dielectric and Calorimetric Studies. *J. Phys. Chem. C* **2016**, *120*, 7373−7380.
(40) Adrjanowicz, K.; Kaminski, K.; Tarnacka, M.; Szklarz, G.; Paluch, M. Predicting Nanoscale Dynamics of a Glass-Forming Liquid from Its Macroscopic Bulk Behavior and Vice Versa. *J. Phys. Chem. Lett.* **2017**, *8*, 696−702.
(41) Rotella, C.; Napolitano, S.; Vandendriessche, S.; Valev, V. K.; Verbiest, T.; Larkowska, M.; Kucharski, S.; Wübbenhorst, M. Adsorption Kinetics of Ultrathin Polymer Films in the Melt Probed by Dielectric Spectroscopy and Second-Harmonic Generation. *Langmuir* **2011**, *27*, 13533−13538.
(42) Serghei, A.; Kremer, F. Metastable States of Glassy Dynamics, Possibly Mimicking Confinement-Effects in Thin Polymer Films. *Macromol. Chem. Phys.* **2008**, *209*, 810−817.
(43) Rotella, C.; Wübbenhorst, M.; Napolitano, S. Probing Interfacial Mobility Profiles via the Impact of Nanoscopic Confinement on the Strength of the Dynamic Glass Transition. *Soft Matter* **2011**, *7*, 5260−5266.
(44) Napolitano, S.; Sferrazza, M. How Irreversible Adsorption Affects Interfacial Properties of Polymers. *Adv. Colloid Interface Sci.* **2017**, *247*, 172−177. Elsevier B.V. September
(45) Napolitano, S.; Rotella, C.; Wübbenhorst, M. Can Thickness and Interfacial Interactions Univocally Determine the Behavior of Polymers Confined at the Nanoscale? *ACS Macro Lett.* **2012**, *1*, 1189−1193.
(46) Perez-de-Eulate, N. G.; Sferrazza, M.; Cangialosi, D.; Napolitano, S. Irreversible Adsorption Erases the Free Surface Effect on the T_g of Supported Films of Poly(4- Tert -Butylstyrene). *ACS Macro Lett.* **2017**, *6*, 354−358.
(47) Napolitano, S.; Capponi, S.; Vanroy, B. Glassy Dynamics of Soft Matter under 1D Confinement: How Irreversible Adsorption Affects Molecular Packing, Mobility Gradients and Orientational Polarization in Thin Films. *Eur. Phys. J. E* **2013**, *36*, 61.
(48) Napolitano, S.; Wübbenhorst, M. The Lifetime of the Deviations from Bulk Behaviour in Polymers Confined at the Nanoscale. *Nat. Commun.* **2011**, *2*, 260.
(49) Laeri, F.; Schüth, F.; Simon, U.; Wark, M. *Host-Guest-Systems Based on Nanoporous Crystals*; Laeri, F., Schüth, F., Simon, U., Wark, M., Eds.; Wiley-VCH: Weinheim, FRG, FRG, 2003.
(50) Iacob, C.; Sangoro, J. R.; Kipnusu, W. K.; Valiullin, R.; Kärger, J.; Kremer, F. Enhanced Charge Transport in Nano-Confined Ionic Liquids. *Soft Matter* **2012**, *8*, 289−293.
(51) Kipnusu, W. K.; Kossack, W.; Iacob, C.; Jasiurkowska, M.; Rume Sangoro, J.; Kremer, F. Molecular Order and Dynamics of Tris(2-Ethylhexyl)Phosphate Confined in Uni-Directional Nanopores. *Z. fur Phys. Chem.* **2012**, *226*, 797−805.
(52) Suzuki, Y.; Duran, H.; Akram, W.; Steinhart, M.; Floudas, G.; Butt, H.-J. Multiple Nucleation Events and Local Dynamics of Poly(ε-Caprolactone) (PCL) Confined to Nanoporous Alumina. *Soft Matter* **2013**, *9*, 9189.
(53) Khassanov, A.; Steinrück, H.-G.; Schmaltz, T.; Magerl, A.; Halik, M.; Khassanov, A.; Steinrück, H.-G.; Schmaltz, T.; Magerl, A.; Halik, M. Structural Investigations of Self-Assembled Monolayers for Organic Electronics: Results from X-ray Reflectivity. *Acc. Chem. Res.* **2015**, *48*, 1901−1908.
(54) Laskowska, M.; Oyama, M.; Kityk, I.; Marszalek, M.; Dulski, M.; Laskowski, L. Surface Functionalization by Silver-Containing Molecules with Controlled Distribution of Functionalities. *Appl. Surf. Sci.* **2019**, *481*, 433−436.
(55) Tu, W.; Ngai, K. L.; Paluch, M.; Adrjanowicz, K. Dielectric Study on the Well-Resolved Sub-Rouse and JG β-Relaxations of Poly(Methylphenylsiloxane) at Ambient and Elevated Pressures. *Macromolecules* **2020**, *53*, 1706−1715.
(56) Alexandris, S.; Papadopoulos, P.; Sakellariou, G.; Steinhart, M.; Butt, H.-J.; Floudas, G. Interfacial Energy and Glass Temperature of Polymers Confined to Nanoporous Alumina. *Macromolecules* **2016**, *49*, 7400−7414.
(57) Kriegs, H.; Meier, G.; Gapinski, J.; Patkowski, A. The Effect of Intramolecular Relaxations on the Damping of Longitudinal and Transverse Phonons in Polysiloxanes Studied by Brillouin Spectroscopy. *J. Chem. Phys.* **2008**, *128*, 014507.

https://doi.org/10.1021/acs.macromol.1c02145
Macromolecules XXXX, XXX, XXX−XXX

(58) Paluch, M.; Casalini, R.; Patkowski, A.; Pakula, T.; Roland, C. M. Effect of Volume Changes on Segmental Relaxation in Siloxane Polymers. *Phys. Rev. E: Stat. Phys., Plasmas, Fluids, Relat. Interdiscip. Top.* **2003**, *68*, 5.
(59) Boese, D.; Momper, B.; Meier, G.; Kremer, F.; Hagenah, J. U.; Fischer, E. W. Molecular Dynamics in Poly(Methylphenylsiloxane) As Studied by Dielectric Relaxation Spectroscopy and Quasielastic Light Scattering. *Macromolecules* **1989**, *22*, 4416−4421.
(60) Adrjanowicz, K.; Winkler, R.; Chat, K.; Duarte, D. M.; Tu, W.; Unni, A. B.; Paluch, M.; Ngai, K. L. Study of Increasing Pressure and Nanopore Confinement Effect on the Segmental, Chain, and Secondary Dynamics of Poly(Methylphenylsiloxane). *Macromolecules* **2019**, *52*, 3763−3774.
(61) Hehre, W. J.; Radom, L.; Schleyer, P. von R.; Pople, J. *AB INITIO Molecular Orbital Theory*; Wiley, 1986.
(62) Frisch, M. J.; Trucks, G. W.; Schlegel, H. B.; Scuseria, G. E.; Robb, M. A.; Cheeseman, J. R.; Scalmani, G.; Barone, V.; Petersson, G. A.; Nakatsuji, H.; et al. *Gaussian 09*; Gaussian, Inc.: Wallingford CT, 2009.
(63) Becke, A. D. Density-Functional Exchange-Energy Approximation with Correct Asymptotic Behavior. *Phys. Rev. A* **1988**, *38*, 3098−3100.
(64) Lee, C.; Yang, W.; Parr, R. G. Development of the Colle-Salvetti Correlation-Energy Formula into a Functional of the Electron Density. *Phys. Rev. B* **1988**, *37*, 785−789.
(65) Weigend, F.; Ahlrichs, R. Balanced Basis Sets of Split Valence, Triple Zeta Valence and Quadruple Zeta Valence Quality for H to Rn: Design and Assessment of Accuracy. *Phys. Chem. Chem. Phys.* **2005**, *7*, 3297.
(66) Ma, H.-z.; Sun, T.-t.; Ye, G.-x. Mean-Square Radius of Gyration and Dipole Moment of Poly(Methylphenylsiloxane) Chains. *Chin. J. Polym. Sci.* **2008**, *26*, 741.
(67) Tu, C.-H.; Zhou, J.; Butt, H.-J.; Floudas, G. Adsorption Kinetics of Cis-1,4-Polyisoprene in Nanopores by In Situ Nanodielectric Spectroscopy. *Macromolecules* **2021**, *54*, 6267−6274.
(68) Tu, C.-H.; Zhou, J.; Doi, M.; Butt, H.-J.; Floudas, G. Interfacial Interactions During In Situ Polymer Imbibition in Nanopores. *Phys. Rev. Lett.* **2020**, *125*, 127802.
(69) Tu, W.; Richert, R.; Adrjanowicz, K. Dynamics of Pyrrolidinium-Based Ionic Liquids under Confinement. I. Analysis of Dielectric Permittivity. *J. Phys. Chem. C* **2020**, *124*, 5389−5394.
(70) Zheng, Y.; Miao, J.; Zhang, F.; Cai, C.; Koh, A.; Simmons, T. J.; Mousa, S. A.; Linhardt, R. J. Surface Modification of a Polyethylene Film for Anticoagulant and Antimicrobial Catheter. *React. Funct. Polym.* **2016**, *100*, 142−150.
(71) Tarnacka, M.; Geppert-Rybczyńska, M.; Dulski, M.; Grelska, J.; Jurkiewicz, K.; Grzybowska, K.; Kamiński, K.; Paluch, M.; Geppert-Rybczynska, M.; Dulski, M.; et al. Local Structure and Molecular Dynamics of Highly Polar Propylene Carbonate Derivative Infiltrated within Alumina and Silica Porous Templates. *J. Chem. Phys.* **2021**, *154*, 064701.
(72) Yu, H. B.; Tylinski, M.; Guiseppi-Elie, A.; Ediger, M. D.; Richert, R. Suppression of β Relaxation in Vapor-Deposited Ultrastable Glasses. *Phys. Rev. Lett.* **2015**, *115*, 185501.
(73) Havriliak, S.; Negami, S. A Complex Plane Representation of Dielectric and Mechanical Relaxation Processes in Some Polymers. *Polymer* **1967**, *8*, 161−210.
(74) Kremer, F.; Schönhals, A. *Broadband Dielectric Spectroscopy*; Springer Berlin Heidelberg: Berlin, Heidelberg, 2003.
(75) Vogel, H. The Law of the Relation between the Viscosity of Liquids and the Temperature. *Phys. Zeitschrift* **1921**, *22*, 645−646.
(76) Fulcher, G. S. Analysis of Recent Measurements of the Viscosity of Glasses. *J. Am. Ceram. Soc.* **1925**, *8*, 339−355.
(77) Tammann, G.; Hesse, W. Die Abhängigkeit Der Viscosität von Der Temperatur Bie Unterkühlten Flüssigkeiten. *Z. Anorg. Allg. Chem.* **1926**, *156*, 245−257.
(78) Adrjanowicz, K.; Kolodziejczyk, K.; Kipnusu, W. K.; Tarnacka, M.; Mapesa, E. U.; Kaminska, E.; Pawlus, S.; Kaminski, K.; Paluch, M. Decoupling between the Interfacial and Core Molecular Dynamics of Salol in 2D Confinement. *J. Phys. Chem. C* **2015**, *119*, 14366−14374.
(79) Adrjanowicz, K.; Kaminski, K.; Koperwas, K.; Paluch, M. Negative Pressure Vitrification of the Isochorically Confined Liquid in Nanopores. *Phys. Rev. Lett.* **2015**, *115*, 265702.
(80) Szklarz, G.; Adrjanowicz, K.; Tarnacka, M.; Pionteck, J.; Paluch, M. Confinement-Induced Changes in the Glassy Dynamics and Crystallization Behavior of Supercooled Fenofibrate. *J. Phys. Chem. C* **2018**, *122*, 1384−1395.
(81) Napolitano, S.; Glynos, E.; Tito, N. B. Glass Transition of Polymers in Bulk, Confined Geometries, and near Interfaces. *Rep. Prog. Phys.* **2017**, *80*, 036602.
(82) Stannarius, R.; Kremer, F.; Arndt, M. Dynamic Exchange Effects in Broadband Dielectric Spectroscopy. *Phys. Rev. Lett.* **1995**, *75*, 4698−4701.
(83) Arndt, M.; Stannarius, R.; Groothues, H.; Hempel, E.; Kremer, F. Length Scale of Cooperativity in the Dynamic Glass Transition. *Phys. Rev. Lett.* **1997**, *79*, 2077−2080.
(84) Politidis, C.; Alexandris, S.; Sakellariou, G.; Steinhart, M.; Floudas, G. Dynamics of Entangled Cis -1,4-Polyisoprene Confined to Nanoporous Alumina. *Macromolecules* **2019**, *52*, 4185−4195.
(85) Arrhenius, S. Über Die Reaktionsgeschwindigkeit Bei Der Inversion von Rohrzucker Durch Säuren. *Z. fur Phys. Chem.* **1889**, *4U*, 226−248.
(86) Pissis, P.; Daoukaki-Diamanti, D.; Apekis, L.; Christodoulides, C. The Glass Transition in Confined Liquids. *J. Phys.: Condens. Matter* **1994**, *6*, L325−L328.
(87) Kremer, F.; Huwe, A.; Arndt, M.; Behrens, P.; Schwieger, W. How Many Molecules Form a Liquid? *J. Phys.: Condens. Matter* **1999**, *11*, A175−A188.
(88) Mel'nichenko, Y. B.; Schüller, J.; Richert, R.; Ewen, B.; Loong, C. -K. Dynamics of Hydrogen-bonded Liquids Confined to Mesopores: A Dielectric and Neutron Spectroscopy Study. *J. Chem. Phys.* **1995**, *103*, 2016−2024.
(89) Williams, G.; Watts, D. C. Non-Symmetrical Dielectric Relaxation Behaviour Arising from a Simple Empirical Decay Function. *Trans. Faraday Soc.* **1970**, *66*, 80−85.
(90) Kohlrausch, R. Theorie Des Elektrischen Rückstandes in Der Leidener Flasche. *Ann. Phys. Chem.* **1854**, *167*, 56−82.
(91) Li, L.; Chen, J.; Deng, W.; Zhang, C.; Sha, Y.; Cheng, Z.; Xue, G.; Zhou, D. Glass Transitions of Poly(Methyl Methacrylate) Confined in Nanopores: Conversion of Three- and Two-Layer Models. *J. Phys. Chem. B* **2015**, *119*, 5047−5054.
(92) Panagopoulou, A.; Napolitano, S. Irreversible Adsorption Governs the Equilibration of Thin Polymer Films. *Phys. Rev. Lett.* **2017**, *119*, 097801.
(93) Wang, H.; Kearns, K. L.; Zhang, A.; Arabi Shamsabadi, A.; Jin, Y.; Bond, A.; Hurney, S. M.; Morillo, C.; Fakhraai, Z.; Arabi Shamsabadi, A.; et al. Effect of Nanopore Geometry in the Conformation and Vibrational Dynamics of a Highly Confined Molecular Glass. *Nano Lett.* **2021**, *21*, 1778−1784.
(94) Tarnacka, M.; Wojtyniak, M.; Brzózka, A.; Talik, A.; Hachuła, B.; Kamińska, E.; Sulka, G. D.; Kaminski, K.; Paluch, M.; Brzózka, A.; Talik, A.; Hachuła, B.; Kaminska, E.; Sulka, G. D.; Kaminski, K.; Paluch, M. Unique´ Behavior of Poly(Propylene Glycols) Confined within Alumina Templates Having a Nanostructured Interface. *Nano Lett.* **2020**, *20*, 5714−5719.

https://doi.org/10.1021/acs.macromol.1c02145
Macromolecules XXXX, XXX, XXX−XXX